Ann. Geophys. Discuss., https://doi.org/10.5194/angeo-2019-57
Manuscript under review for journal Ann. Geophys.
Discussion started: 29 April 2019

Annales Geophysicae Discussions
Open Access
EGU

Comparing high-latitude thermospheric winds from FPI and CHAMP accelerometer measurements

Anasuya Aruliah[1], Matthias Förster[2], Rosie Hood[1], Ian McWhirter[1], Eelco Doornbos[3,4]

[1]Atmospheric Physics Laboratory, University College London, Gower Street, London, WC1E 6BT, UK
[2]Helmholtz-Zentrum Potsdam, GFZ German Research Centre for Geosciences, Telegrafenberg, 14473 Potsdam, Germany
[3]Old affiliation: Faculty of Aerospace Engineering, Delft University of Technology (TU Delft), Kluyverweg 1, 2629 HS Delft, The Netherlands
[4]Current affiliation: Royal Netherlands Meteorological Institute (KNMI), Utrechtseweg 297, 3731 GA De Bilt, The Netherlands

Correspondence to: Anasuya Aruliah (a.aruliah@ucl.ac.uk) and Matthias Förster (mfo@gfz-potsdam.de)

Abstract. It is generally assumed that horizontal wind velocities are independent of height above the F_1-region (> 300 km) due to the large viscosity of the upper thermosphere. This assumption is used to compare two completely different methods of thermospheric neutral wind observation, using two distinct locations in the high-latitude Northern Hemisphere. The measurements are from ground-based Fabry-Perot Interferometers (FPI), and from in-situ accelerometer measurements onboard the CHAMP satellite, which was in a near polar orbit. The UCL KEOPS FPI is located in the vicinity of the auroral oval at the ESRANGE site near Kiruna, Sweden (67.8°N, 20.4°E). The UCL Longyearbyen FPI is a polar cap site, located at the Kjell Henriksen Observatory on Svalbard (78.1°N, 16.0°E). The comparison is done in a statistical sense, comparing a longer time series obtained during nighttime hours in the winter months (November to January); with overflights of the CHAMP satellite between 2001 and 2007 over the observational sites, within ±2° (±220 km horizontal range). The FPI is assumed to measure the line-of-sight winds at ~240 km height, i.e. the peak emission height of the atomic oxygen 630.0 nm emission. The cross-track winds are derived from state-of-the-art precision accelerometer measurements at altitudes between 450 km (in 2001) to 330 km (in 2007); i.e. 100-200 km above the FPI wind observations. We show that CHAMP winds at high latitudes are systematically 1.5-2 times larger than FPI winds. In addition to testing the consistency of the different measurement approaches, the study aims to clarify the effects of viscosity on the height dependence of thermospheric winds.

1 Introduction

Global circulation models (GCM) of the upper atmosphere (80-600 km altitude) appear in two forms: climatologies based on empirical measurements, and theoretical models that calculate the atmospheric conditions using the principles of physics and chemistry. These models are important for space weather studies and are also applied in understanding and predicting drag on low-altitude satellites, space debris, and the study of re-entry of near Earth objects. The theoretical and empirical models rely on observations from ground-based instruments around the world and global observations by satellites to provide constraints and boundary conditions. In particular, models must account for energy from sources external to the upper atmosphere (i.e., direct solar radiation, particle precipitation and heat flow from above; radiative, conductive and convective

Ann. Geophys. Discuss., https://doi.org/10.5194/angeo-2019-57
Manuscript under review for journal Ann. Geophys.
Discussion started: 29 April 2019

heating from below; the magnetospheric electrodynamic driver at high-latitudes), which is divided between acceleration of the gas and heating. The empirical evidence for the energy budget is provided by observations of winds and temperatures.

The use of accelerometers on satellites to measure thermospheric winds had previously been reported quite rarely (Marcos and Forbes, 1985; Forbes et al., 1993). Over the last few years CHAMP and GOCE winds have been reported (e.g. Förster et al., 2008; Doornbos et al., 2010). The advantage of this technique consists in the fairly direct in-situ measurement, with relatively high spatial (temporal) resolution, of the cross-track wind component along the orbital track with only a limited number of special assumptions for the data interpretation. Adding more satellites (e.g., GRACE and GRACE-FO), should allow better full wind vector reconstructions in terms of statistical averages (Förster et al., 2008; Förster et al., 2017) as well as parameterized statistical studies of the upper thermosphere dynamics in the near future. As a result, it makes it imperative that the derived winds are correct because satellites provide global coverage of the upper atmosphere, unlike the small number of ground-based instruments currently in existence. The larger databases and global coverage of the satellites will particularly influence a semi-empirical model such as the Horizontal Wind Model (Drob et al., 2015), which is commonly used as a climatology of winds to provide initial boundary conditions and validation for physics-based global circulation models (GCMs).

In this paper we show that upper thermospheric winds measured by the CHAMP satellites are systematically 1.5 to 2 times larger than those measured by ground-based Fabry-Perot Interferometers (FPIs) at an auroral site and polar cap site. It is imperative to know whether this discrepancy is real (i.e. there is a variation of speed with respect to height), or whether we have uncovered a problem of the absolute scaling of wind measurements by comparing FPIs with CHAMP. With incorrect scaling, there arises a problem of distortion of energy budget calculations of the upper atmosphere as demonstrated below.

Consider a simple argument where the added energy per unit volume is δE, and the wind measured by the satellite and FPI are U_{sat}, and U_{FPI}, respectively. The energy is redistributed between a change in kinetic energy and heating of the atmosphere. If the gas has density ρ, and is accelerated from being initially stationary to speed U, then the energy redistribution is given by Eq. (1)

$$\delta E = \frac{1}{2}\rho U^2 + \rho C_p \delta T \quad (1)$$

Let us assume that the satellite and FPI are measuring the same volume of gas, but are not absolutely calibrated. Let δT_{sat} and δT_{FPI} be the change in temperature due to heating as measured by the satellite and FPI, respectively. Thus the change in energy is given by Eq. (2), assuming a mean density ρ during this process.

$$\delta E = \frac{1}{2}\rho U_{sat}^2 + \rho C_p \delta T_{sat} = \frac{1}{2}\rho U_{FPI}^2 + \rho C_p \delta T_{FPI} \quad (2)$$

Ann. Geophys. Discuss., https://doi.org/10.5194/angeo-2019-57
Manuscript under review for journal Ann. Geophys.
Discussion started: 29 April 2019

Annales Geophysicae Discussions

Consider if the measurements from the satellite and FPI are such that $U_{sat} = 2U_{FPI}$, i.e. either the satellite or the FPI (or both) are wrongly calibrated, then substituting for U_{sat} in Eq. (2), and rearranging both equations, leads to Eq. (3).

$$4\delta T_{FPI} - \delta T_{sat} = \frac{3\delta E}{\rho C_p} \tag{3}$$

Thus Eq. (3) demonstrates that for positive δE (i.e. heating), the inferred satellite temperatures are larger than the FPI temperatures (e.g. if $\delta E \approx 0$, then $\delta T_{sat} \approx 4\delta T_{FPI}$). In other words, the satellite wind measurements imply that more energy is put into heating the gas, and less into accelerating the gas, while the FPI measurements would indicate the reverse. This would result in a mismatch between modelled and observed temperature changes. The FPI can measure temperatures to test this, as will be done in a future study. The temperature discrepancy would also have a knock-on effect on the calculation of density ρ of the gas as determined by the satellites, or by ground-based FPIs, since $\delta\rho = nk_B\delta T$, where k_B is the Boltzmann constant and n is the number density of the gas particles. Note that this argument for a point measurement is oversimplified. Owing to the high viscosity and heat conductivity, the whole air column above the measurement location should be accelerated and heated.

2 The CHAMP accelerometer data

The challenging mini-satellite payload (CHAMP) was managed by the GFZ German Research Centre for Geosciences of the Helmholtz Centre Potsdam. This mission was designed to perform detailed studies of the Earth's gravitational and magnetic field with unprecedented accuracies and space/time resolutions as well as GPS atmosphere and ionosphere profiling. The spacecraft was launched in July 2000 into a circular near-polar orbit with 87.3° inclination at an initial altitude of ~460 km (Reigber et al., 2002). Its orbital altitude gradually decayed to ~400 km in 2003 and ~330 km in 2008, and ended in September 2010.

One key scientific instrument onboard CHAMP was a triaxial accelerometer. It was located at the spacecraft's center of mass and effectively probed the in-situ air drag. Thermospheric mass density and cross-track neutral wind can be obtained from the drag acceleration observations. It is very difficult to determine the error estimate because it depends on several variables as discussed in Doornbos et al. (2010) and shown in Table 5 from Visser et al. (2019). This indicates that for force-derived winds, the largest sensitivity is to energy accommodation, which is of the order of several tens of ms^{-1}.

A first analysis of the high-latitude thermospheric wind circulation in dependence on the IMF orientation was performed by Förster et al. (2008) using the preliminary methodology of cross-track wind estimations from accelerometer data as described in Liu et al. (2006). Förster et al. (2011) then presented an overview of the average transpolar thermospheric circulation in terms of the vorticity. Here, they made use of the newly

Ann. Geophys. Discuss., https://doi.org/10.5194/angeo-2019-57
Manuscript under review for journal Ann. Geophys.
Discussion started: 29 April 2019

Annales Geophysicae Discussions

calibrated and re-analysed data set that resulted from an ESA study, initiated for the Swarm satellites mission launched in November 2013 (Helleputte et al., 2009).

As pointed out by Doornbos et al. (2010), the along-track wind is not resolvable because it induces a similar signal in the acceleration as the density variation. This wind component is ignored, or the value from an empirical wind model is used, because the along-track wind is a relatively small magnitude in comparison with the satellite speed of 7.6 km s^{-1}. The empirical wind model used is, for example, HWM90 (Hedin et al., 1991) or its latest edition HWM14, as published by Drob et al. (2015). In polar areas the along-track wind velocity can achieve up to 10% of the satellite speed. Consequently, the along-track mass density estimation can have an error of about 20% in the polar latitudes, because the acceleration is proportional to the wind velocity squared (e.g., Doornbos et al., 2010). But it is less easy to estimate the error in the cross-track wind in the polar region due to considerably smaller acceleration signals. There are also systematic contributions from other sources such as gas-surface interactions, surface properties, spacecraft shape, spacecraft attitude and radiation pressure accelerations, which make the satellite aerodynamic coefficients difficult to resolve (see Doornbos et al., 2010, and the error budget in Appendix A of that paper; Mehta et al., 2017 and March et al., 2018). The pre-processed data of the accelerometer were re-sampled to 10-sec averages for the further use in this study. Measurements of 10-sec cadence correspond to a spatial separation of 76 km or about 2/3° in latitude between the individual data points.

3 The Fabry-Perot Interferometer data

The advantage of using Fabry-Perot Interferometers is that they make direct measurements of thermospheric wind speeds using only a few instrumental or geophysical assumptions. They are also generally reliable instruments that can be left to run for months at a time. The FPIs operated by University College London are located at the Kiruna Esrange Optical Platform System (KEOPS) in northern Sweden; and on the island of Svalbard at the Adventdalen Observatory (before November 2006), from which it was moved to the Kjell Henriksen Observatory (after November 2006). The geographic and geomagnetic coordinates of these two stations are given in Table 1 for Kiruna (KEOPS) and Table 2 for Longyearbyen (Svalbard). The Altitude-Adjusted Corrected Geomagnetic Coordinates (AACGM) are obtained from http://sdnet.thayer.dartmouth.edu/aacgm/aacgm_calc.php#AACGM (Shepherd, 2014). A date of 15 December 2002 was used, for an altitude of 240 km. Owing to the large field-of-view of the FPIs (see later) the locations of the volumes observed by the FPIs in the East and West look directions are also given, and the corresponding MLT.

Ann. Geophys. Discuss., https://doi.org/10.5194/angeo-2019-57
Manuscript under review for journal Ann. Geophys.
Discussion started: 29 April 2019

148 **Table 1**

FPI Site	Geographic coordinates	AACGM geomagnetic coordinates for 15 Dec 2002 at 240 km altitude	AACGM magnetic local time (MLT) midnight in UT
Kiruna (KEOPS)	67.87°N, 21.03°E	65.08°N, 103.32°E	1.860 hrs
Kiruna (KEOPS) EAST	67.87°N, 26.6°E	64.8°N, 107.8°E	2.16 UT
Kiruna (KEOPS) WEST	67.87°N, 15.5°E	65.4°N, 98.9°E	1.57 UT

149

150 **Table 2**

FPI Site	Geographic coordinates	AACGM geomagnetic coordinates for 15 Dec 2002 at 240 km altitude	AACGM magnetic local time (MLT) midnight in UT
Longyearbyen (KHO after 2006)	78.15°N, 16.04°E	75.38°N, 111.80°E	2.43 UT
Longyearbyen EAST (KHO after 2006)	78.15°N, 33.6°E	74.4°N, 123.6°E	3.21 UT
Longyearbyen WEST (KHO after 2006)	78.15°N, -1.5°E	76.8°N, 100.3°E	1.66 UT
Longyearbyen (Advendalen before 2006)	78.19°N, 15.92°E	75.43°N, 111.80°E	2.43 UT
Longyearbyen EAST (Advendalen before 2006)	78.19°N, 33.5°E	74.4°N, 123.6°E	3.21 UT
Longyearbyen WEST (Advendalen before 2006)	78.19°N, -1.7°E	76.9°N, 100.3°E	1.66 UT

151

152 A significant limitation of ground based FPIs is that optical measurements of airglow and aurora at
153 thermospheric altitudes are only possible during the night when the sun's zenith angle is greater than 98°. This
154 means that the high latitude FPI observing season runs only in the winter months: from September to April at
155 KEOPS; and October to March at Longyearbyen. The FPIs have been nearly continually observing the 630 nm
156 emission from airglow and aurora every winter night since 1981 and 1986, respectively. Complete 24 hours of
157 observation are possible during November to January at Longyearbyen. Thermospheric winds have been
158 monitored by calculating the Doppler shifts of the 630nm airglow radiation intensities. The FPI instrument has a
159 mirror that rotates to look in several directions (e.g.north, north-east, east, south, west, north-west, zenith and a
160 calibration lamp) to provide line-of-sight wind measurements at a fixed elevation angle. The exposure times can
161 be as low as 10 seconds, up to 120 seconds. A typical complete scan cycle takes ~4 minutes for Kiruna and ~5

mins for Longyearbyen. After 1999, when laser calibrations were made possible, thermospheric temperatures were measured from the thermal broadening of the emission line. More details of operation may be found in Aruliah et al. (2005) and references therein.

The 630nm emission has a peak intensity at an altitude of around 240 km. So measurements of the Doppler shifts and thermal broadening of the emission line are used to determine the winds and neutral temperatures of the upper thermosphere (> 200km altitude). The elevation angle of the mirror is 45° for the Kiruna FPI and 30° for the Longyearbyen FPI. Thus the radius of the field-of-view is 240 km and 416 km, respectively, which represents roughly a 5° and 8° separation in latitude of the north and south viewing volumes at the respective sites. At these high latitudes where the magnetospheric dynamo dominates the plasma flows, ion-neutral coupling can create meso-scale structures in the upper thermosphere on horizontal scale sizes of as little as ~100 km (e.g. Aruliah et al., 2001, Emmert et al., 2006a). So average wind speeds have been determined for each of the 4 cardinal look directions in order that the meso-scale structure is not lost. The winds are strongly dependent on UT, season, solar cycle and geomagnetic activity due to the dominant forcing mechanisms of pressure gradients and ion-neutral coupling in the high latitude upper thermosphere. The maximum average wind vector magnitudes measured by an FPI at Kiruna were shown to be in the range 100-300 ms^{-1} and the errors of measurements were around 10-20 ms^{-1} (Aruliah et al., 1996). The main sources of error are:

a) Poor signal to noise when the 630 nm intensities are low, such as at solar minimum, or geomagnetically quiet conditions.

b) The existence of large vertical winds. These break the assumption that the winds are predominantly horizontal. Vertical winds are generally small, but can be a few 10s of ms^{-1} at high latitudes (Aruliah and Rees, 1995; Ronksley, 2016). Large vertical winds introduce an error of a few per cent into the calculation of a horizontal wind component from the line-of-sight measurement.

c) The assumption that the neutral winds are nearly constant with respect to altitude above 200 km owing to the very low density and consequently high viscosity of the upper thermosphere.

The altitude distribution of the 630 nm emission has a peak emission altitude of between 220-250 km (e.g. Link and Cogger, 1988; Vlasov et al., 2005). However, the emission profile also has a full width at half maximum intensity of around 50-70 km, i.e. sampling altitudes tens of km below and above the emission peak. The ground-based FPI observes a height-integration of the emission along the line-of-sight. The measured Doppler shift is therefore an integration of the Doppler shifts at all altitudes, weighted by the emission profile. However, there are several reasons to justify why we are confident that the FPI provides a good sample of the winds at ~240 km altitude. The excited atomic oxygen state in the O (^1D-^3P) transition is a forbidden transition with a long life-time of ~110 sec (Bauer, 1973), which allows the atom to thermalise before emission and be representative of the surrounding gas. Below 200 km the molecular composition increases significantly, and the long lifetime means that the 630 nm emission is quenched due to molecular collisions with N_2 and O_2. Consequently we can assume there is minimal contribution of Doppler shifts from below 200 km altitude, which is a region where the neutral wind magnitude has a large height dependence (note that the winds at 100 km altitude are a few tens of ms^{-1} while at 250 km altitude are a few hundreds of ms^{-1}). Above the altitude of the

Ann. Geophys. Discuss., https://doi.org/10.5194/angeo-2019-57
Manuscript under review for journal Ann. Geophys.
Discussion started: 29 April 2019

emission peak the flux falls off rapidly with altitude and also with distance from the FPI, which minimises the contribution of winds from the region above. Overall it is suggested that the FPI measured winds may underestimate the winds at ~240 km altitude by no more than about 10% due to the contribution of winds below the peak emission height.

4 CMAT2 model winds

The UCL Coupled Middle Atmosphere Thermosphere (CMAT2) model is a 3-dimensional, time-dependent physics-based model, that solves numerically the non-linear coupled continuity equations of mass, momentum and energy (Harris et al., 2002). The model has a latitude resolution of 2°, longitude 18°, and a one third scale height for a height range of ~15 km (top of the troposphere) to 300-600km (top of the thermosphere). Thermospheric heating, photodissociation and photoionisation are calculated for solar X-ray, EUV and UV radiation between 0.1-194 nm (Fuller-Rowell, 1992; Torr et al, 1980a and 1980b; Roble, 1987). High latitude ionospheric parameters of ion and electron densities and temperatures, plus field-aligned plasma velocities, are from the Coupled Sheffield University High-latitude Ionosphere Model (Quegan et al., 1982; Fuller-Rowell et al., 1996). The high latitude auroral precipitation is provided by the TIROS/NOAA auroral precipitation model (Fuller-Rowell and Evans, 1987) and the high latitude electric field model is from Foster et al., (1986). Other features are detailed in Harris et al. (2002). The CMAT2 winds will be presented as part of the discussion below.

5. Results

Data were chosen from the 3-year periods 2001-2003 and 2005-2007, when the CHAMP satellite was in orbit. These represent periods of solar maximum and minimum, respectively. CHAMP data were collected all year around, but the FPI data were limited to nighttime periods only.

5.1 CHAMP average winds

Figures 1 and 2 show plots of average CHAMP accelerometer measurements of the cross-track thermospheric wind component during the whole period of years 2001–2003, that were obtained during direct overflights above the FPI stations at Longyearbyen (Figure 1) and KEOPS (Figure 2). The cross-track wind component is defined as pointing into positive y-direction of the S/C coordinate system with its x axis along the orbital trace, the z axis toward nadir, and the y-axis completing the right-hand system. The y-wind component therefore points perpendicular to the orbital plane to the right side, when looking in the direction of flight. Given the high inclination (87.3°) of the CHAMP satellite, this corresponds approximately to the geographically eastward direction for the ascending orbital track (blue lines in Figure 1) except for very high geographic latitudes (see below). The cross-track wind measurements of the descending orbital tracks (red lines) have been flipped in sign to get nearly the same eastward wind component.

Figure 1a and 2a show average values for all data, while Figures 1b, 1c, 2b and 2c show the summer and winter averages. There are many more data points for the Longyearbyen station, at a higher geographic latitude compared with KEOPS. This confirms the fact that the relative probability of overhead crossings of high-

latitude stations by low Earth orbiting (LEO) satellites with a near-polar circular orbit augments with increasing latitude. A statistical study has to make some compromise with respect to the area of accepted local coincidences of the satellite recordings above the ground-based observations and also with regard to the further data binning. Here, a circular area with 2° radius and hourly bins versus local time have been used which produces a sufficiently good coverage. Further binnings have been been tested to investigate the effect on the results. A shorter radius deteriorates the statistics within the bin, while larger bins tend to smear the spatial and temporal variations. Data filtering with respect to other parameters like, e.g., season, solar wind and interplanetary magnetic field (IMF) values, solar radiation and geomagnetic activity indices should be taken into account if they appear to make a significant effect.

The variance of the cross-track neutral wind magnitude is considerably larger during the whole day above the station at higher latitudes. The average phase of the diurnal eastward wind variation differs also considerably between the data sets of the two observatories. The eastward wind maximizes during the pre-midnight hours over Longyearbyen, while a smaller maximum and a shorter interval of eastward wind is seen at lower latitudes above the KEOPS station (2–3 hours versus about 6 hours). The eastward neutral thermospheric wind is approximately sinusoidal for Longyearbyen (Fig. 1a), but reveals two maxima/minima over the KEOPS station (Fig. 2a). The westward wind maximizes there at about 19 LT and prior to midday (~11 LT). Finally, the variance of the cross-track neutral wind magnitude over the lower latitude station KEOPS is relatively large during the afternoon to early nighttime hours (~15–20 LT). This might be due to the position of this station relative to the large dusk cell which is known to be strongly dependent on, in particular, the IMF By component (cf., e.g., Rees et al., 1986; Killeen et al., 1995; Förster et al., 2008 and Förster et al., 2011). In contrast to KEOPS, the higher latitude station Longyearbyen is located close to or even poleward of the dusk cell's focus, so that the cross-polar cap circulation of the neutral thermospheric air dominates.

Ann. Geophys. Discuss., https://doi.org/10.5194/angeo-2019-57
Manuscript under review for journal Ann. Geophys.
Discussion started: 29 April 2019

Annales Geophysicae Discussions
Open Access
EGU

261 **Figure 1: CHAMP observations over Longyearbyen during solar maximum 2001-2003. a) All data – ascending (blue)**
262 **and descending (red) averages; b) Summer (May-Aug) and c) Winter (end Oct-early Mar).**

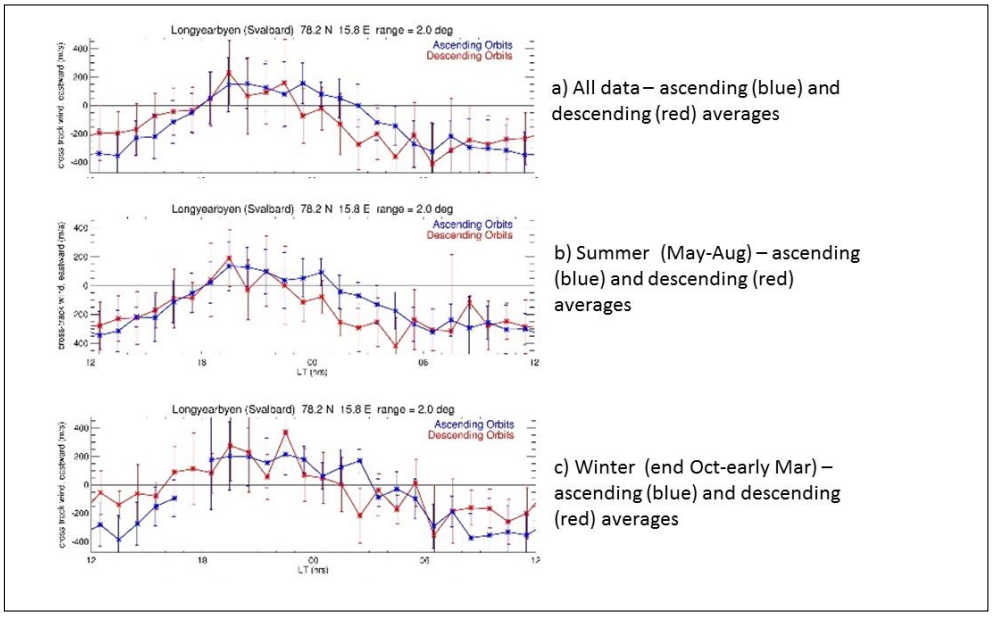

263

264 **Figure 2: CHAMP observations over KEOPS during solar maximum 2001-2003. a) All data – ascending (blue) and**
265 **descending (red) averages; b) Summer (May-Aug) and c) Winter (end Oct-early Mar).**

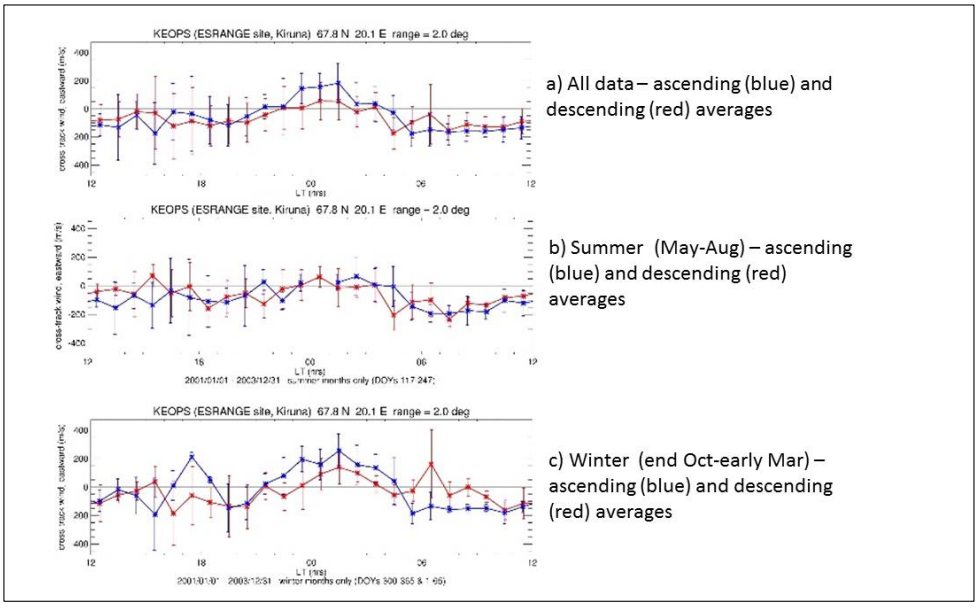

Figures 1b and 1c repeat the statistical plot of Fig. 1a for Longyearbyen for the years 2001-2003 with high solar activity, but confined to the winter and summer months, respectively. Similarly for Figures 2b and 2c for KEOPS. The statistical significance is therefore reduced, in particular for the KEOPS station, but seems to be still sufficient. The winter recordings (Fig. 1c and 2c) during nighttime hours can directly be compared with the FPI observations (Figs. 5 and 6).

The principle behaviour of the Longyearbyen and KEOPS eastward wind component is similar to that for the full year coverage, but there are also obvious seasonal differences. The wind component amplitudes, in particular the eastward maxima, are smaller during summer compared with the winter months, while the phases are almost the same. The statements about the variance of the eastward/westward wind component for both stations that have been made with respect to the full year statistics in Fig. 1 hold also for both winter and summer plots, maybe with slightly larger values for the winter months.

The ascending and descending orbits are analyzed separately in their statistical behaviour (blue and red lines and vertical bars, respectively), and show distinct differences. This points to the problem of co-alignment of the ascending and descending orbital tracks (despite the simple sign flip). The small offset of ~2.7° from a strict polar orbit of the satellite causes some deviation from the east/westward pointing of the cross-track measurements. At low to mid-latitudes, the deviation from purely geographically eastward direction corresponds in good approximation to this colatitude angle of the satellite's inclination $\beta \approx 2.7°$, but at high latitudes and in particular near the poles it can deviate considerably. This non-alignment angle α (deviation from purely eastward) can be estimated in dependence on the observer's colatitude θ with spherical angle relations using a simplified spheric geometry of the Earth as in Eq. (4).

$$\alpha = \arcsin\left(\frac{\sin\beta}{\sin\theta}\right) \tag{4}$$

Using the geographic coordinates of the observatories in Table 1, one gets an α-angle of 7.2° and 13.3° for KEOPS and Longyearbyen, respectively. The angular difference ($2\cdot\alpha$) between the two one-component cross-track wind measurements of the ascending and descending orbital tracks is already considerable for the most northward station at Longyearbyen and this offset can be noticed in, for example, Figure 1a as an offset between the wind averages for ascending and descending orbital tracks during certain intervals, where the wind component perpendicular to the zonal wind direction, i.e. the north-south meridional wind, is large. This is obviously the case for the nighttime hours between 23–05 LT and the daytime hours between ~10–17 LT for Longyearbyen and for a few nighttime hours between 23–03 LT for the KEOPS FPI station.

If the FPI technique, in particular the tri-static measurements for certain periods (Aruliah et al.,2005; Griffin et al., 2008), allow the determination of specified neutral wind directions, one might consider comparing the wind magnitudes for the descending and ascending orbital tracks separately for an eastward $\pm\alpha$ orientation, respectively. Here, one should note, that at an observation point with an even higher geographic latitude (ideally at ~86.2° geographic latitude, where the two branches of one-component observations would be perpendicular

Ann. Geophys. Discuss., https://doi.org/10.5194/angeo-2019-57
Manuscript under review for journal Ann. Geophys.
Discussion started: 29 April 2019

304 to each other) it would in principle be possible to derive the full thermospheric wind vector from the cross-track
305 accelerometer measurements. This is, strictly spoken, valid in a statistical mean with characteristic times of a
306 few days, i.e. with the repetition period of ascending and descending orbits over one and the same high-latitude
307 location.
308
309 The meridional component is much larger than the zonal one during considerable periods of the nighttime
310 observation. So, to minimize the error in comparing the neutral wind magnitude, it would be better to compare
311 the full vectors. Already a small error of the measurement orientation could make a large effect on the relatively
312 small eastward wind component, which could lead us to wrong conclusions about the characteristics of the
313 differences between FPI and CHAMP accelerometer measurements. The offset between the geographic and
314 geomagnetic coordinates allows the construction of the full vector plots as statistical averages taken over a
315 period of at least 131 days of CHAMP's precession period in order to cover all local times. This statistical
316 mapping is limited to magnetic latitudes poleward of about > 60° for both hemispheres (cf. Förster et al., 2008).
317

318 **Figure 3: CHAMP observations over Longyearbyen during solar minimum 2005-2007. a) All data – ascending (blue)**
319 **and descending (red) averages; b) Summer (May-Aug) and c) Winter (end Oct-early Mar).**

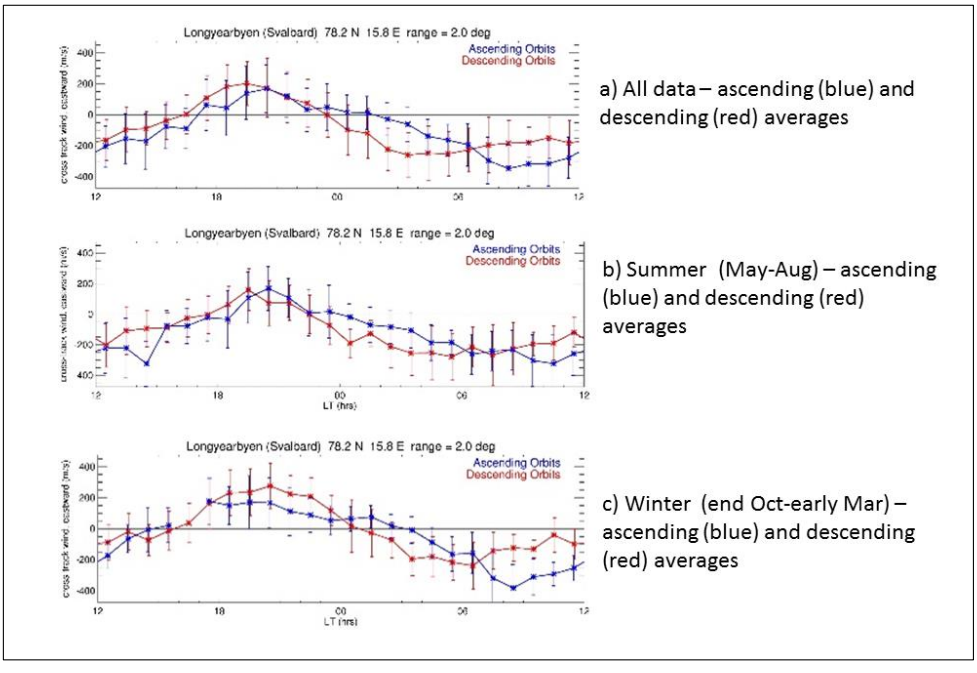

320

Ann. Geophys. Discuss., https://doi.org/10.5194/angeo-2019-57
Manuscript under review for journal Ann. Geophys.
Discussion started: 29 April 2019

Annales Geophysicae Discussions

Figure 4: CHAMP observations over KEOPS during solar minimum 2005-2007. a) All data – ascending (blue) and descending (red) averages; b) Summer (May-Aug) and c) Winter (end Oct-early Mar).

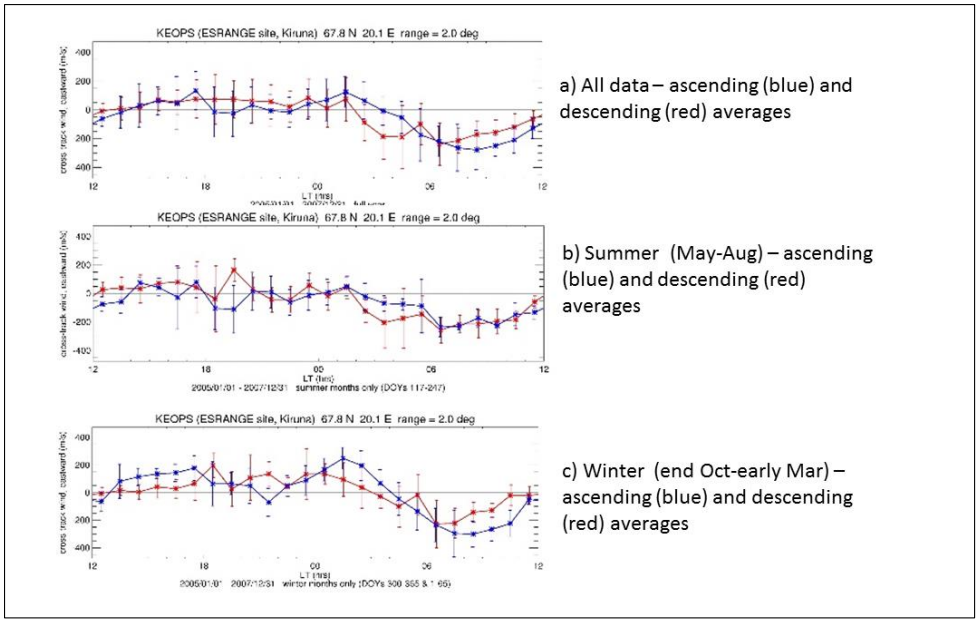

Figures 3 and 4 show the corresponding plots to Figs. 1 and 2, but now for low solar activity conditions during the years 2005-2007. They reveal some differences as, e.g., generally smaller amplitudes and different wind phases. Here, the zonal wind above KEOPS seems to point eastward during most times of the day except the morning hours 04–11 LT.

5.2 FPI average winds

The average winds observed at Kiruna and Longyearbyen are presented in Figures 5 and 6. Local Time is 1 hour ahead of Universal Time for both sites. The format of these figures is that the plots 5a, 5c, 6a and 6c show the average zonal wind component, comparing observations to the East and West of the site. The plots 5b, 5d, 6b and 6d show the average meridional wind component from the North and South look directions. The full set of cardinal direction measurements, are presented to provide a context for the comparison with the zonal wind measurements made by CHAMP, especially since the CHAMP y-axis is only roughly zonal. The standard error of the mean ε is added as an error bar to the East and North data, where $\varepsilon = \sigma/\sqrt{(N\text{-}1)}$, σ is the standard deviation and N is the number of data points. The periods of data cover the winter months of 2001-2003 and 2005-2007 to match with the CHAMP datasets. The FPIs cannot measure winds during cloudy periods owing to the scatter of light by the clouds, and are only able to observe the emission during the hours of darkness. Thus the observing days cannot be identical to the dates when CHAMP passed overhead of the two sites. Longyearbyen has 24 hours of darkness during the months of November to January, so there are nearly 24 hours of observations, but

the longest period of darkness at Kiruna is around 18 hours in mid-winter. CHAMP, meanwhile, is able to provide a full 24 hours of observations from drag measurements.

There are consistent differences in the winds observed to the geographic East and West, or to the North and South. This is understandable because the Kiruna site is, on average, at the equatorward edge of the auroral oval, while Longyearbyen is at the poleward edge. The expansion and contraction of the auroral oval during an active period means that the northern half of the FPI field-of-view can be very different from the southern half. In fact, Emmert et al. (2006b) have shown that high latitude neutral winds are better ordered in geomagnetic coordinates of magnetic latitude and magnetic local time than in geographic coordinates and universal time. The AACGM geomagnetic coordinates shown in Tables 1 and 2 give an indication of how different are the magnetic latitudes for the East and West look directions.

Figure 5 shows average zonal and meridional winds from FPI observations at Longyearbyen. Figs 5a and 5b show solar maximum years (2001-2003), while 5c and 5d show solar minimum years (2005-2007). Figs 5a and 5c show the zonal winds to the East and West using the convention of +East, while Figure 5b and 5d shows the meridional winds to the North and South, using +North.

Ann. Geophys. Discuss., https://doi.org/10.5194/angeo-2019-57
Manuscript under review for journal Ann. Geophys.
Discussion started: 29 April 2019

Annales Geophysicae Discussions

359 **Fig 5 FPI winter average wind components at Longyearbyen for geomagnetically quiet conditions (0<Kp<2). The**
360 **standard error of the mean is shown for one example component. Solar maximum (2001-2003) a) zonal, b) meridional**
361 **average winds. Solar minimum (2005-2007) c) zonal, d) meridional average winds. North and East are purple lines,**
362 **while South and West are light blue.**

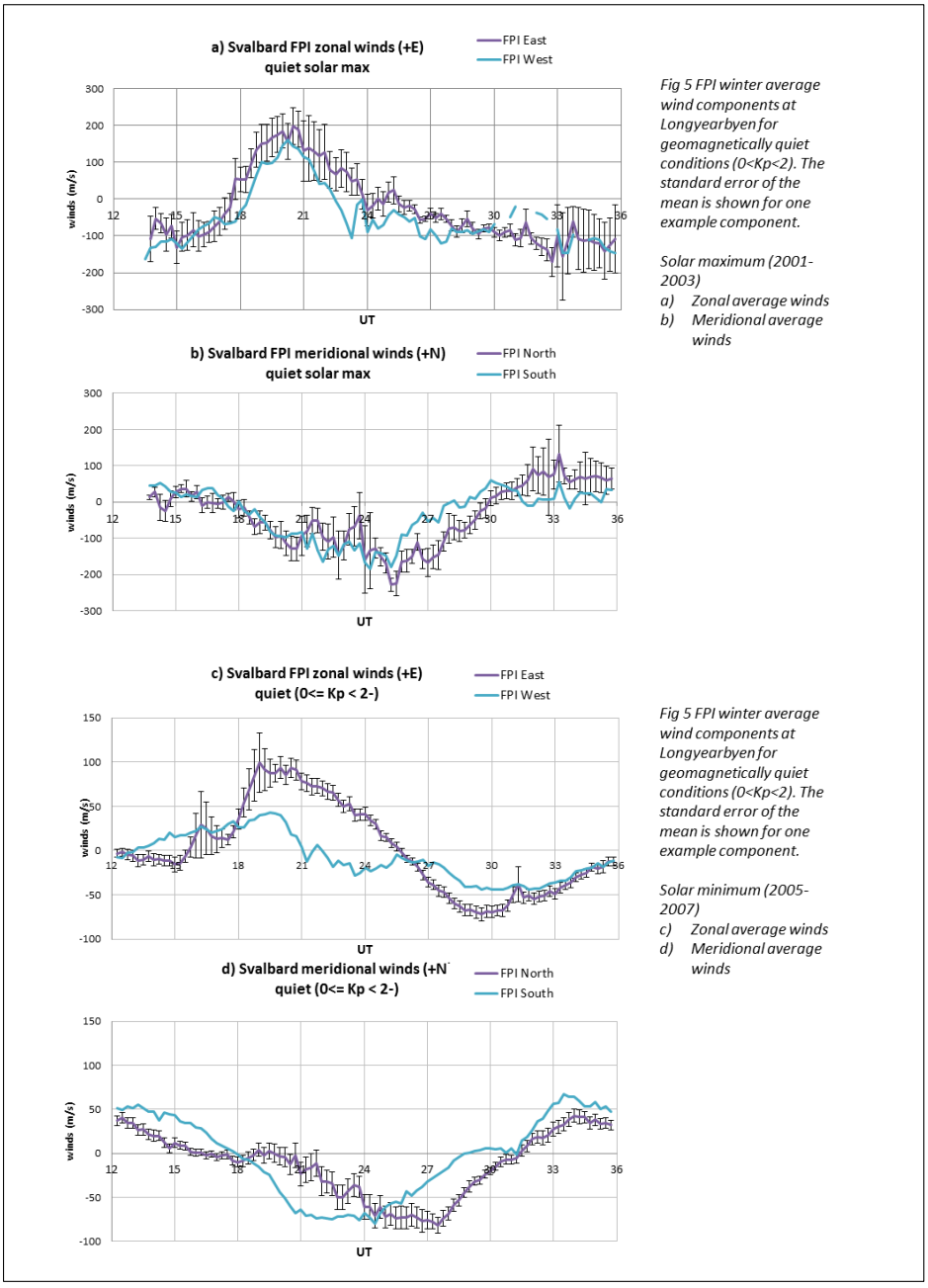

Fig 5 FPI winter average wind components at Longyearbyen for geomagnetically quiet conditions (0<Kp<2). The standard error of the mean is shown for one example component.

Solar maximum (2001-2003)
a) Zonal average winds
b) Meridional average winds

Fig 5 FPI winter average wind components at Longyearbyen for geomagnetically quiet conditions (0<Kp<2). The standard error of the mean is shown for one example component.

Solar minimum (2005-2007)
c) Zonal average winds
d) Meridional average winds

Ann. Geophys. Discuss., https://doi.org/10.5194/angeo-2019-57
Manuscript under review for journal Ann. Geophys.
Discussion started: 29 April 2019

Annales Geophysicae Discussions
Open Access
EGU

Longyearbyen is just within the polar cap. The winds are predominantly antisunward despite the geomagnetic activity level, since this is the direction for both the pressure gradient and ionospheric convection. As a result, Longyearbyen observations are a somewhat less obvious indicator of ion-neutral coupling behaviour than observations at KEOPS in the period 1800-2100 UT. The Longyearbyen solar maximum (2001-2003) winter winds (day numbers 300-65), during geomagnetically quiet conditions ($0 \leq Kp < 2o$) are shown in Figures 5a and 5b. The zonal winds (Figure 5a) show westward winds before 1800 UT and then eastward winds for ~6 hours which then turn westward. The maximum wind speed is about 200 ms^{-1} eastward between 1800-2400 UT. The meridional winds (Figure 5b) are slightly northward before 1700 UT, then turn southward until 0600 UT, and return northward. The maximum speed is about 200 ms^{-1} southward at about 0100 UT. The standard errors of the mean are around ±30 ms^{-1}, however the values vary systematically through the night. Between 1800-2100 UT the standard error is around 3 times larger than between 0300-0900 UT when it is very small.

Figures 5c and 5d show the Longyearbyen FPI winds for clear nights during winter (DOY 300-65) 2005-2007, geomagnetically quiet conditions ($0 \leq Kp < 2o$). There is a full 24 hours of observations in this dataset, and the extreme quiet of this solar minimum period has provided a large number of observations for this category. The antisunward flow appears clearly. There is a strong phase lag between the observations to the North and South. This is puzzling because it cannot be explained in terms of ordering high latitude winds in geomagnetic coordinates. This category is for the most geomagnetically quiet conditions possible: solar minimum during a prolonged solar minimum, and the lowest Kp values. Under these conditions the geographic coordinate system under which the solar flux heating operates, should be the most appropriate. The standard errors of the mean are very small, around ±10 ms^{-1}, though again there is a systematic trend. Between 2100-0300 UT the standard error of the meridional wind is about 2-3 times larger than at other times. Between 1500-2000 UT the zonal wind standard error becomes considerably larger.

Ann. Geophys. Discuss., https://doi.org/10.5194/angeo-2019-57
Manuscript under review for journal Ann. Geophys.
Discussion started: 29 April 2019

Annales Geophysicae Discussions

Fig 6 FPI winter average wind components at KEOPS for geomagnetically quiet conditions (0<Kp<2). The standard error of the mean is shown for one example component. Solar maximum (2001-2003) a) zonal, b) meridional average winds. Solar minimum (2005-2007) c) zonal, d) meridional average winds. North and East are purple lines, while South and West are light blue.

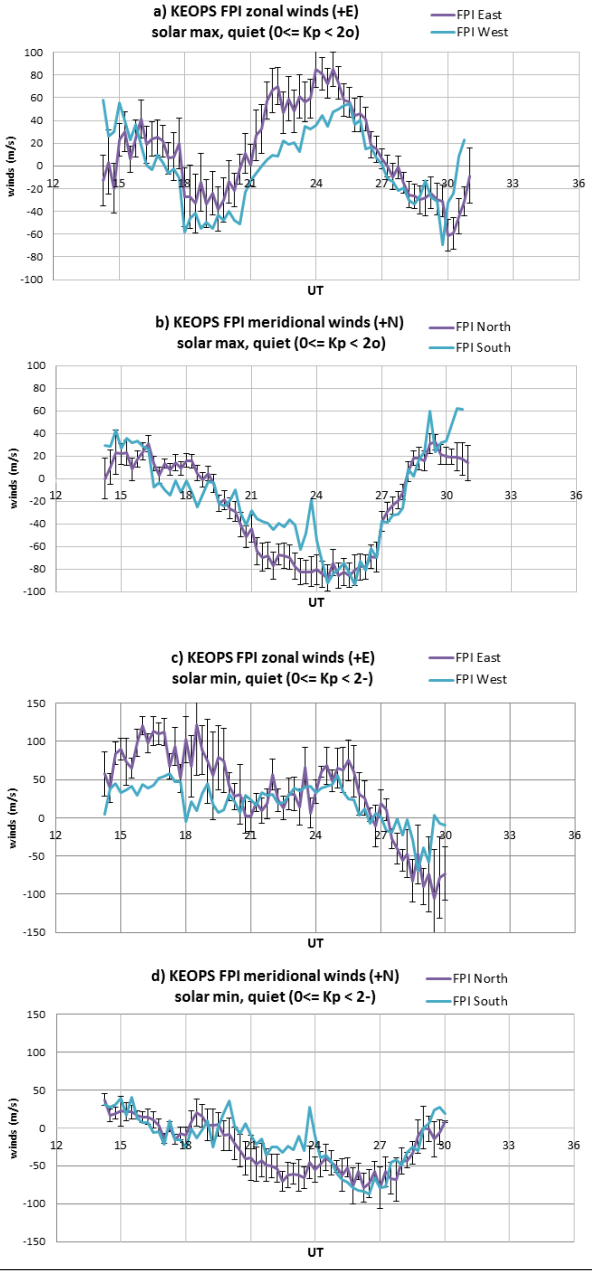

Fig 6 FPI winter average wind components at KEOPS for geomagnetically quiet conditions (0<Kp<2). The standard error of the mean is shown for one example component.

Solar maximum (2001-2003)
a) Zonal average winds
b) Meridional average winds

Fig 6 FPI winter average wind components at KEOPS for geomagnetically quiet conditions (0<Kp<2). The standard error of the mean is shown for one example component.

Solar minimum (2005-2007)
c) Zonal average winds
d) Meridional average winds

Ann. Geophys. Discuss., https://doi.org/10.5194/angeo-2019-57
Manuscript under review for journal Ann. Geophys.
Discussion started: 29 April 2019

Annales Geophysicae Discussions

Figure 6 shows the KEOPS FPI winds for clear nights during winter (DOY 300-65) geomagnetically quiet conditions ($0 \leq Kp < 2o$). The general diurnal trends are similar for both solar maximum (Figs 6a,b) and minimum (Figs 6c,d). The meridional winds show antisunward flow that is predominantly driven by the pressure gradient from dayside EUV heating, resulting in fairly weak southward winds reaching a maximum value of nearly 100 ms^{-1}. The standard errors of the mean are around ±10-15 ms^{-1}. The zonal winds are eastward before 1800UT, reaching a maximum speed of a few 10s ms^{-1}. After 1800UT the zonal winds turn westward for a few hours and back eastwards around 2100UT. Between 2100-0300 UT the zonal winds reach their maximum speed of up to 80 ms^{-1} before turning westward again. The zonal winds are more variable, and their standard errors of the mean are larger than for the meridional winds, at around ±20-30 ms^{-1}.

The few hours of westward flowing zonal winds during 1800-2100 UT are particularly interesting (Figs 6a and 6c). The westward flow indicates that the winds are briefly under the influence of the clockwise dusk cell of ionospheric convection. Through collisions between the ions and neutral gas, momentum is transferred to the neutrals, which diverts them from the direction of the pressure gradient driven anti-sunward/eastward flow. The action of the centrifugal force balancing the Coriolis force keeps the winds entrained in the cell (Fuller-Rowell and Rees, 1984). As the KEOPS site passes under the region of the Harang Discontinuity (Harang, 1946), the FPI West zonal winds turn back to eastward about 40 mins after the FPI East zonal winds. This is because the KEOPS FPI East observing volume is a horizontal distance of 480 km away from the FPI West volume (note that the distance between the viewing volumes depends on the altitude of the 630 nm emission). However, note that at the latitude of KEOPS, the time taken for the Earth to rotate through a distance of 480 km is 46 mins. The difference between 40 min and 46 min is partly due to the difference in magnetic latitude. It is also due to the Harang Discontinuity being dependent on the IMF B_y orientation, resulting in a smearing out of the MLT interval.

Figures 6c and 6d show the KEOPS FPI winds for clear nights for the years 2005-2007 during winter (day numbers 300-65), geomagnetically quiet conditions ($0 \leq Kp < 2o$). These years were during the unusually extended solar minimum of the last solar cycle when the solar flux levels were extremely low, and observations of aurora were rare. Consequently the plasma density was smaller, and the thermosphere was more compressed, resulting in smaller neutral densities at a given height. Under these conditions the ion drag driver is less efficient, and the pressure gradients, together with the Coriolis and centrifugal forces, play a larger role. Thus, although the trends are similar to the solar maximum winds; the zonal winds are strongly eastward throughout the evening sector. There are no westward zonal winds until after 0300 UT, and generally the wind amplitudes are smaller. The maximum meridional wind is about 80 ms^{-1} southward around 0300 UT. The maximum zonal winds are seen to the East, and these are around 100 ms^{-1} eastward in the evening sector and start to increase westwards towards 100 ms^{-1} by 0600 UT. The standard errors of the mean are around ±30 ms^{-1}, which are larger than for solar maximum conditions.

The general trends seen in the CHAMP zonal winds are also seen in the FPI winds. The phases match extremely well for both (a) Longyearbyen and (b) KEOPS. However, there is a considerable difference in magnitude. The average ratio of the zonal wind magnitudes (CHAMP /FPI) for Longyearbyen is 1.8, and for KEOPS is 3.3.

Ann. Geophys. Discuss., https://doi.org/10.5194/angeo-2019-57
Manuscript under review for journal Ann. Geophys.
Discussion started: 29 April 2019

Annales Geophysicae Discussions
Open Access
EGU

Fig 7 Longyearbyen (Svalbard) winters 2001-2004, 2<Kp<4: average zonal winds measured using CHAMP and FPI, including standard errors of the mean. These are compared with FPI winds in 1980 and the HWM87 and HWM90 model winds from Hedin et al (1991).

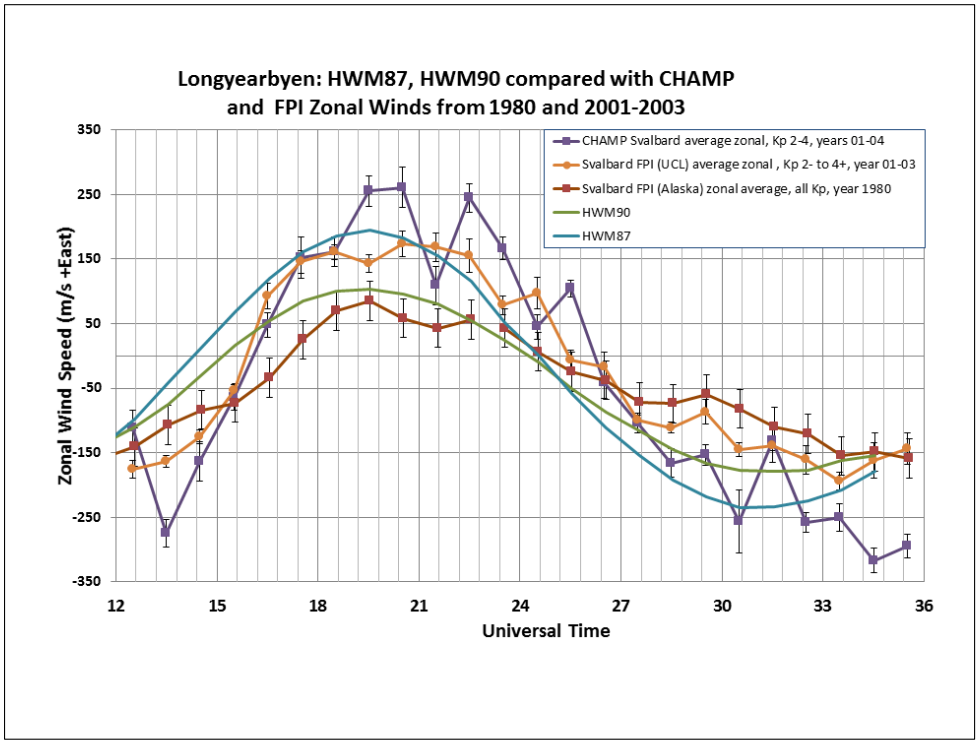

Figure 7 is a direct comparison from several different sources of Longyearbyen zonal winds. These represent moderately active conditions (2 < Kp < 4) during winter months (November to January) for solar maximum years that are 20 years apart. CHAMP cross-track winds were collected during the years 2001-2004, while the UCL Longyearbyen FPI observations were during 2001-2003 (a failure occurred in the rotating mirror mechanism in late December 2003). The CHAMP data are the averages of the ascending and descending orbits. Values taken from Figure 9 in the paper by Hedin et al. (1991) are also plotted. These values are measurements from the University of Alaska FPI collected in 1980, 1981 and 1983; and the HWM87 and HWM90 model. The U.Alaska FPI winds are an average of the East and West look directions, justified by the assumption of a uniform horizontal wind field. This was a common practice at that time owing to the longer exposure times of the earlier FPIs (6-12 minutes) which used photomultipliers with piezoelectrical scanning of the FPI etalon gap size in order to view the full Free Spectral Range (Deehr et al., 1980). For Figure 7, only the UCL Longyearbyen FPI East direction winds are shown (Figure 8a shows both East and West look directions). The UCL FPIs were amongst the first FPIs to use fixed gap etalons to image the full FSR onto a 2D array of pixels. This allowed shorter exposure times, and a rapid cycle of look directions. During the 1980s and 1990s we used state-of-the-art UCL designed and built Imaging Photon Detectors (McWhirter et al., 1981) and then EMCCDs (Andor iXon 887/885) were installed around 2005 (McWhirter, 2008). The revolution over the last 30 years in

low light detectors has allowed observations with exposure times as little as 10 seconds at auroral latitudes (Ford et al., 2007).

All sources show generally similar phases, with peak eastward winds in the evening sector, between 18-24UT and westward winds in the morning sector, between 06-12UT, as expected for anti-sunward flows. Table 2 shows that the AACGM MLT for Longyearbyen is about 2.4 (± 0.8 for the East and West volumes) hours ahead, so magnetic midnight is approximately at 21.6 UT. The standard errors of the mean are plotted for all data. The U.Alaska Longyearbyen FPI standard deviations are around ± 150 ms^{-1}, which are similar to the UCL FPI. For the purposes of comparison, a standard error of ±30 ms^{-1} is plotted for the U.Alaska FPI data, similar to the average UCL FPI standard error. It was noted in the Hedin et al (1991) paper that for both hemispheres, the average high latitude winds from the FPIs at Sondrestrom, Longyearbyen and College in the northern hemisphere, and Mawson in the southern hemisphere, showed a systematically smaller diurnal variation than the DE 2 mass spectrometer data. The HWM87 model was based on satellite data from the DE 2 and AE-E satellites. Consequently, the addition of the FPI and incoherent scatter radar datasets to the HWM90 database resulted in a smaller diurnal variation compared with the HWM87 winds. The more recent measurements from CHAMP and the UCL FPI are clearly systematically different in magnitude, but consistent with the trend noticed by Hedin et al (1991) for satellite wind measurements to be larger than from ground-based FPIs. The diurnal amplitude of the UCL zonal winds is about 170 ms^{-1}, and for the U.Alaska winds is about 125 ms^{-1}. The CHAMP zonal winds are systematically the largest in magnitude, with a diurnal amplitude of around 300 ms^{-1}.

The average of the monthly F10.7 fluxes is 193 for the winter periods Nov-Jan of 1980-81, 1981-82 and 1983-84, and 170 for the winters of 2001-2003. Yet despite the higher average solar flux in 1980, the UCL FPI zonal wind magnitudes have a significantly larger amplitude than the U.Alaska zonal winds. Closer inspection of the 3 winter periods of 2001-2003 shows a spike in the average monthly F10.7 for November 2001-January 2002 (i.e. <F10.7> is 168 for Nov-Jan 2001-2002; 219 for Nov-Jan 2002-2003; and 152 for Nov-Dec 2003) which may account for the 3 winter average UCL FPI winds being larger than for U.Alaska. The geomagnetic activity levels are similar, averaging Kp values in the range 3- to 3o for all three winters.

Ann. Geophys. Discuss., https://doi.org/10.5194/angeo-2019-57
Manuscript under review for journal Ann. Geophys.
Discussion started: 29 April 2019

Annales Geophysicae Discussions
Open Access
EGU

473 **Fig 8a Comparison of CHAMP and FPI measurements of Longyearbyen (Svalbard) zonal average winds, including**
474 **standard errors of the mean, for winters 2001-2004. Plus comparison with Alaska 1980 from Hedin et al. (1991). Fig**
475 **8b Comparison of CHAMP and FPI measurements of KEOPS zonal average winds, including standard errors of the**
476 **mean, for winters 2001-2004.**

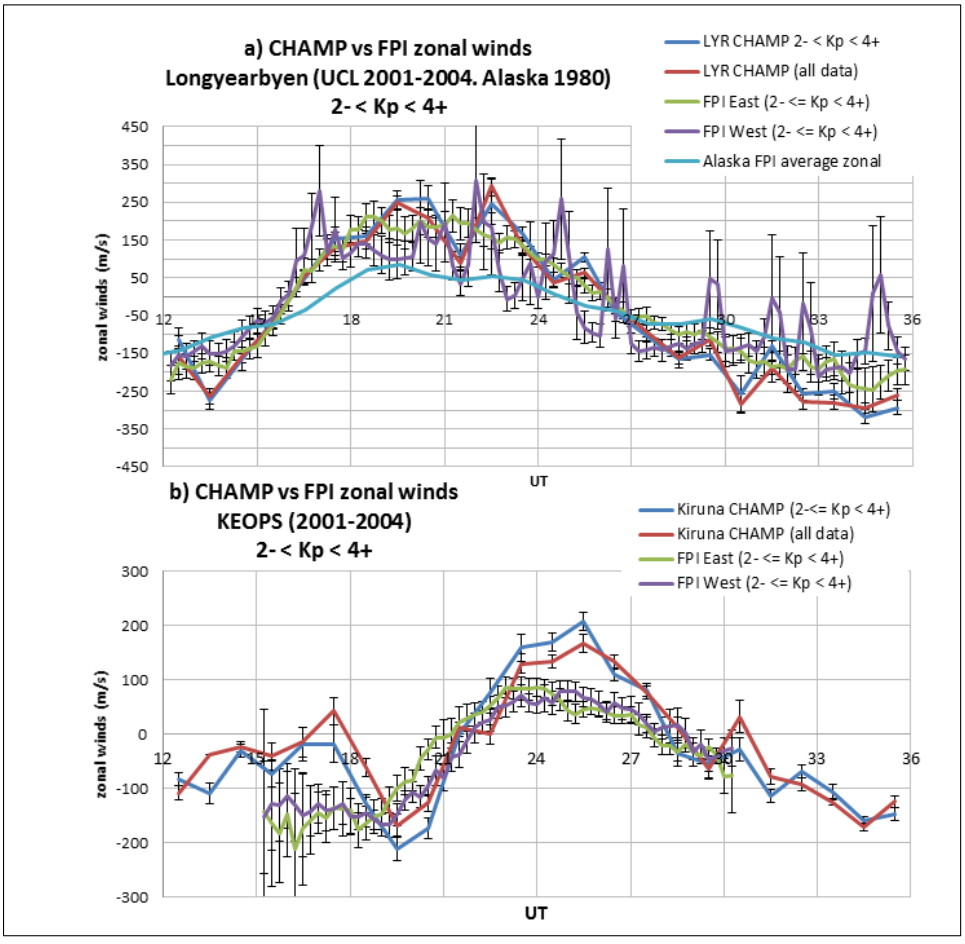

477

478 Figure 8a and 8b show a comparison of the CHAMP zonal winds against the UCL FPI winds for the winters of
479 2001-2004. At Longyearbyen there is 24 hour coverage by the FPI owing to continual darkness between
480 November-January (Figure 8a). The FPI and CHAMP data are selected for moderately active conditions (2- <
481 Kp < 4+) as in Figure 7. Here the UCL FPI West look direction is added. Also plotted are CHAMP data for all
482 activity levels. The Alaska average of East and West look directions from 1980-1983 completes the plot.
483 Overall there is a very close agreement in phase between the CHAMP and FPI zonal winds. However, there is a
484 noticeable difference between the UCL FPI East and West look directions. Table 2 shows that the AACGM
485 magnetic latitude of Longyearbyen West volume is nearly 2° further poleward than the East volume, which

Ann. Geophys. Discuss., https://doi.org/10.5194/angeo-2019-57
Manuscript under review for journal Ann. Geophys.
Discussion started: 29 April 2019

results in weaker emissions and larger error bars. In addition there is a small phase shift owing to the different magnetic coordinates as discussed further in the next paragraph.

At Kiruna the hours of darkness are between 15-06UT for the period November-January. The UCL FPI average zonal winds for 2- < Kp < 4+ are shown separately for the East and West look directions in Figure 8b. There is a smaller difference between these look directions than for the Longyearbyen zonal winds. The evening winds for moderately active solar maximum conditions are around -150 ms^{-1} (westward), and reach a peak of around 70 ms^{-1} (eastward) in the midnight sector. The AACGM MLT for Kiruna is about 1.9 (± 0.3 for the East and West volumes) hours ahead, so magnetic midnight is approximately at 22.1 UT, which is the time separating the period of the evening eastward electrojet and the morning westward electrojet in magnetic local time coordinates. The behaviour of the zonal winds shows strong ion-neutral coupling for these moderately active conditions, so that there is a semidiurnal variation representative of the twin cell ionospheric convection pattern at auroral latitudes. This is in addition to the day-night diurnal variation of winds driven by the pressure gradient.

The phase of the CHAMP zonal winds is in good agreement, but the amplitude is considerably larger. The peak evening wind reaches -200 ms^{-1} (westward) and 200 ms^{-1} (eastward) by 02 UT. What is particularly interesting about this comparison is the difference between the CHAMP and FPI winds in the period 15-20 UT. The CHAMP winds are considerably less westward, and are more similar to FPI average zonal winds for geomagnetically quieter conditions at solar maximum, as shown in Figure 6a. The large standard error of the mean during the period 15-20 UT shows how sensitive the winds are to ion drag within the dusk cell.

Fig 9 Frequency distribution of the ratios of CHAMP/FPI one-hour averaged zonal winds observed in the winter period Nov-Jan for 2001-2004 for Svalbard (red) and Kiruna (blue).

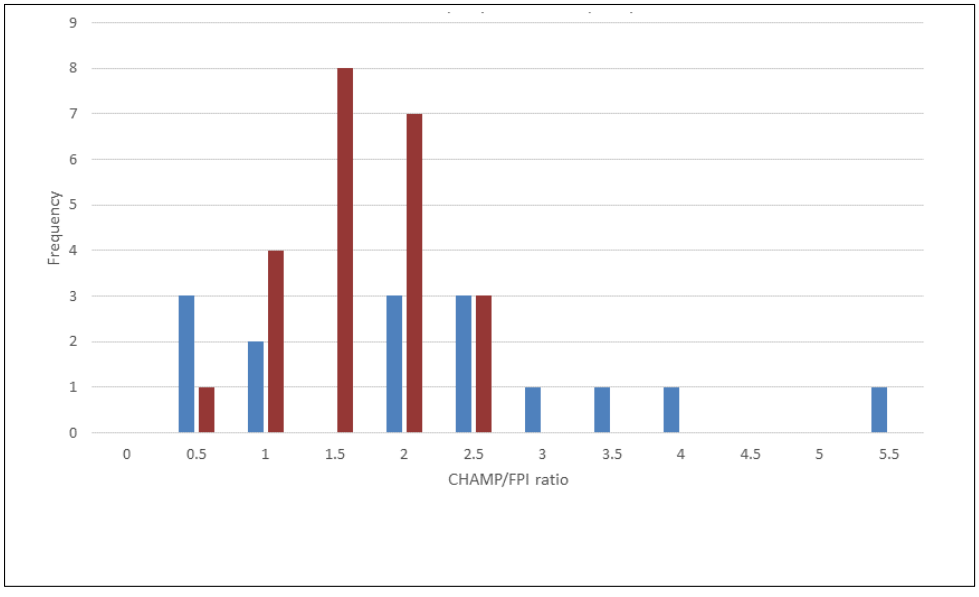

Figure 9 shows a histogram of the frequency distribution of the ratios of CHAMP/FPI average zonal wind magnitudes observed in the winter period Nov-Jan for 2001-2004 for Kiruna and Longyearbyen. The UCL FPI zonal winds observed to the East and West have been averaged into 1 hour bins to match the CHAMP averages of the ascending and descending zonal winds. The Longyearbyen ratios cluster in the range 1.0 - 2.5, while the Kiruna ratios are more widely spread. Overall there is a general trend for the satellite wind magnitudes to be larger by a factor of 1.5 - 2.0.

6. Discussion

We have shown that there is a similar phase, but a considerable difference between the average zonal wind magnitudes measured by the CHAMP satellite and the ground-based FPIs for a polar cap and auroral site. Our premise is that the large viscosity of the upper thermosphere should minimise any vertical structure in the winds above around 250 km altitude. The difference in wind magnitudes could have various explanations. It could be that A) we are mistaken about the vertical structure of winds; or B) that there is a problem with the scaling of the two methods of measurement; or C) the measurement procedures introduce differences, e.g. in-situ versus remote integration; comparison of different spatial and/or temporal resolutions. There may be other, unexpected, reasons for the mainly amplitude differences in the measurements.

With respect to hypothesis A: the CHAMP satellite zonal winds are of a similar magnitude to the original GOCE satellite winds (Liu et al., 2016 and Visser et al., 2019), and to the UCL CMAT2 model simulations. However, while the CHAMP satellite altitude was between 350-400 km, the GOCE satellite had an unusually low altitude around 250 km, which was close to the FPI 630 nm emission peak altitude. The CMAT2 winds are typical of values from other GCMs, which were largely calibrated against measurements by satellites in the 1970s and 1980s, in particular the DE-2 satellites. Killeen et al (1984) found a good agreement between the FPI at Longyearbyen (then called the University of Ulster FPI, and subsequently the University of Alaska FPI) for observations in December 1981. This is because the DE-2 satellite measurements were made using the Wind and Temperature Spectrometer (WATS), rather than derived from satellite drag measurements. The DE-2 satellite flew from August 1981 to February 1983, which means that the average monthly F10.7 flux included some of the highest solar flux values of the last 30 years. This may account for why the GCMs have such large wind values.

With respect to hypothesis B: the satellite drag community are aware of a scaling issue. Defining the drag coefficient is the largest source of error. Bruinsma et al (2014) had to multiply GOCE densities by a factor of 1.29 to match the real-time High Accuracy Satellite Drag Model (Storz et al., 2005). HASDM uses data assimilation from the orbits of 75-85 inactive payloads and debris over 200-900 km altitude that are tracked by the Space Surveillance Network (SSN) and is considered a benchmark by that community. Recently March et al. (2019), reanalysed thermospheric densities derived from very precise satellite accelerometers and GPS acceleration using high fidelity satellite geometries. The densities for all the spacecraft surveyed were greater than those derived using surfaces defined by flat panels; and more consistent with each other. The CHAMP and GOCE densities were found to be 11% and 9% larger. Although there is no simple link between densities and winds, this re-scaling of densities gives an indication that it may be necessary to scale winds down for the same measured acceleration (see section 6.3 and Eq. 6).

Ann. Geophys. Discuss., https://doi.org/10.5194/angeo-2019-57
Manuscript under review for journal Ann. Geophys.
Discussion started: 29 April 2019

Annales Geophysicae Discussions
Open Access
EGU

546 **6.1 Considering the viscosity of the upper thermosphere**

547 Let us first consider hypothesis A, that the CHAMP and ground-based FPI average zonal measurements are both
548 correct, and that the factor of 1.5-2.0 difference in wind magnitudes is due to the 100-150 km difference in the
549 altitude of the measurements. Conventional fluid dynamics theory predicts that the viscosity is very high in the
550 upper thermosphere owing to the very low particle densities at these altitudes. The viscosity of a fluid
551 determines how resistant it is to shear forces that cause adjacent layers to move at different speeds. Turbulent
552 viscosity dominates the atmosphere below about 100 km, but molecular viscosity dominates the upper
553 atmosphere. The viscosity of the upper thermosphere is very large, and in the CMAT2 model the molecular
554 viscosity η, is given by Eq. (5) (Harris, 2001) which is based on Dalgarno and Smith (1962) and Banks and
555 Kockarts (1973).

556 $$\eta = 4.5e^{-5} \times \left(\frac{T}{1000}\right)^{0.71} \quad (5)$$

557 As a consequence of large viscosity, there is little shear between the different altitude layers above ~200 km for
558 both winds and neutral temperatures (hence the name thermosphere representing an iso-therm behaviour). The
559 issue raised in this paper is that the difference between CHAMP and FPI wind magnitudes is too large to be
560 consistent with the assumption of large viscosity over this range of altitudes.

561

Ann. Geophys. Discuss., https://doi.org/10.5194/angeo-2019-57
Manuscript under review for journal Ann. Geophys.
Discussion started: 29 April 2019

Annales Geophysicae Discussions
Open Access
EGU

562 **Fig 10 CMAT2 zonally averaged zonal winds for 00UT at December solstice 2008 (solar minimum conditions) to**
563 **demonstrate the effect of drastically reducing the molecular viscosity in order to raise the altitude where winds**
564 **become independent of altitude. The left panel shows isobars for a standard simulation, while the right panel**
565 **represents a simulation where the molecular viscosity is 100 times smaller.**
566

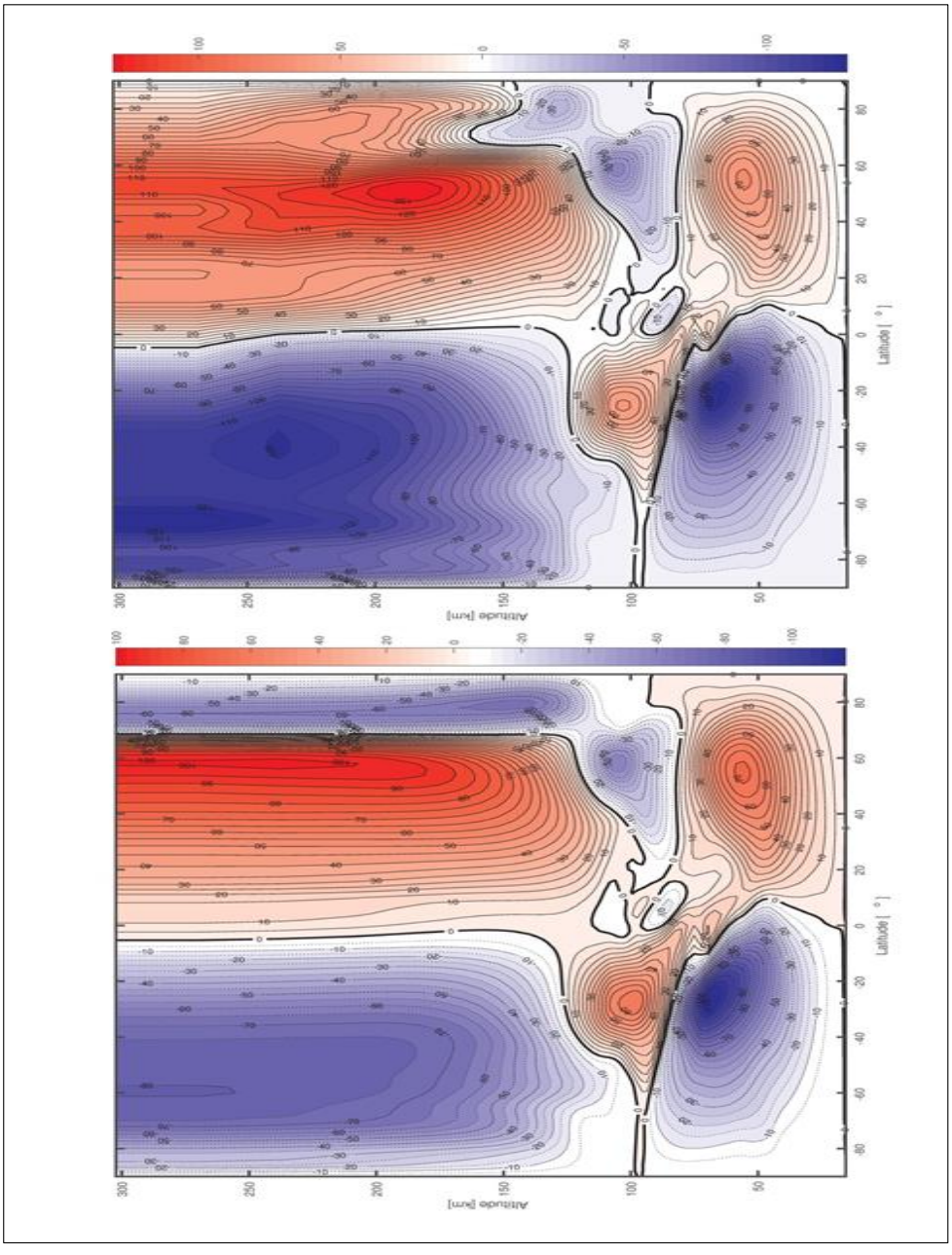

Figure 10 shows two versions of the CMAT2 zonally averaged zonal winds for 00 UT for December solstice 2008 (solar minimum conditions). These are latitude-height plots, where the height is from 15 km to 300 km. From about 250 km the contour lines become near vertical because the large molecular viscosity of the upper thermosphere minimises the shear in the winds. The left hand plot is the standard run using standard values of molecular viscosity. The right hand plot shows the contours for a simulation where the molecular viscosity has been reduced by a factor of 100. The variation of the molecular viscosity with respect to temperature (and consequently height for our purposes) has been tested theoretically and experimentally by Dalgarno and Smith (1962), and the factor of 100 is an unrealistic extreme used to test the model. The consequence is that the height at which contours become vertical is raised to closer to 280 km. This is a small difference and certainly does not account for the apparent vertical gradient indicated by the difference between the CHAMP and FPI zonal winds.

Song et al. (2009) studied the local response of the ionosphere and thermosphere to changes of the magnetospheric convection at polar latitudes on the basis of a 1-D three-fluid model approach. It includes ions, electrons, and neutral particles and their collisions within the polar cap, hence describing the coupled processes between the magnetosphere, ionosphere, and thermosphere in the vertical direction along the magnetic flux tubes. In this self-consistent 1-D solution, the neutral wind speed is obtained as a function of height. The model describes the dynamic response of the ionosphere/thermosphere after relatively rapid changes of the magnetospheric convection within about 10-20 Alfvèn wave travel times (or 15-30 minutes) within the magnetosphere between conjugated hemispheres, or between the ionosphere and the magnetopause, until the system reaches its steady state again. It is shown that the fastest acceleration of the neutrals occurs near 350 km in the F layer, where the effective neutral-ion collision frequency maximizes (see Figs. 6 and 7 of Song et al., 2009). Considering the dynamic character of frequent changes of the IMF and the magnetospheric convection, the stronger accelerations at F2 layer heights could result in temporary vertical neutral wind gradients. However, the 1-D model approach neglects forces due to neutral pressure and effective viscosity in the 3-D continuum of the upper thermosphere (Song et al., 2009). To describe correctly the long-range coupling on time scales from longer than few seconds to less than 30 min, the inductive effect (Faraday's law) as well as the dynamic effect of the neutrals, in particular (acceleration terms), need to be considered (Song and Vasyliunas, 2013). This poses a challenge for future modelling efforts of the M-I-T system.

Recently Vadas and Crowley (2017) published results from observations of 10 Travelling Ionospheric Disturbances at ~283 km altitude, observed in 2007 with the TIDDBIT ionospheric sounder near Wallops Island, USA. They used ray tracing on the TIDs and simultaneously measured a peak in the neutral wind at ~325 km altitude using a sounding rocket. They found a serious discrepancy between where the gravity waves were predicted to dump energy using conventional dissipative theory, and the observations from TIDDBIT and the rocket. Conventional theory predicted that all the gravity waves should have dispersed at a scale height below the rocket measurement. Consequently they have proposed that the molecular viscosity should not increase as rapidly with altitude above 220 km. This may account for some of the difference between the CHAMP and FPI zonal winds and will need to be tested in future modelling studies.

Ann. Geophys. Discuss., https://doi.org/10.5194/angeo-2019-57
Manuscript under review for journal Ann. Geophys.
Discussion started: 29 April 2019

Annales Geophysicae Discussions

6.2 FPI Doppler shift to wind speed procedure

Hypothesis B is that the FPI and/or CHAMP observations may need to be re-scaled. To start with the FPIs we will look at the calculation of the Doppler shift and then at the height integration procedure of a ground-based FPI.

The calculation of the wind speed requires few assumptions, though the process of fitting the FPI fringes is more complicated (e.g. Makela et al., 2011). The wind speed u is determined from the Doppler shift of the wavelength $\Delta\lambda$ of the moving volume of gas which emits at wavelength λ, where the free-space wavelength is λ_o and the speed of light c (Eq. 7).

$$\lambda = \lambda_o\left(1+\frac{u}{c}\right) = \lambda_o + \Delta\lambda \tag{7}$$

The speed of the volume of gas u is given by Eq. (8), which is proportional to the ratio of the Doppler shift in fringe peak position (in bins) Δx; and the free spectral range (FSR), Δx_{FSR}. The FSR is the equivalent wavelength shift to shift a fringe from overlapping one order of the baseline wavelength λ_o, to the next order. The other terms in Eq. (8) are the refractive index μ of the medium between the etalon plates and the separation of the plates, d (Hecht and Zajak, 1980).

$$u = \left(\frac{\Delta x}{\Delta x_{FSR}}\right)\left(\frac{c\lambda_o}{2\mu d}\right) \tag{8}$$

The etalon gap is evacuated so μ=1, and the other parameters are known. Thus for example, for an etalon gap d = 10 mm, emission λ_o = 630 nm, free spectral range Δx_{FSR} = 150 bins, a Doppler shift of 1 bin (Δx = 1 bin) would represent a wind of 63 ms^{-1}.

All the parameters for the scaling of the FPI winds in this equation are known. There is the issue of determining the zero Doppler shift baseline because there is no laboratory source of the excited atomic oxygen. However, the method used to determine the baseline (i.e., using a helium-neon source with the assumption that the vertical component of the wind is negligible) introduces an average systematic offset error of at most 10-20 ms^{-1}, which is small compared with horizontal wind magnitudes (Aruliah and Rees, 1995).

Ann. Geophys. Discuss., https://doi.org/10.5194/angeo-2019-57
Manuscript under review for journal Ann. Geophys.
Discussion started: 29 April 2019

Fig 11 left: height profile of CMAT2 zonal winds at Svalbard. Right: height profile of the red line emission intensity profile from the Vlasov et al (2005) model.

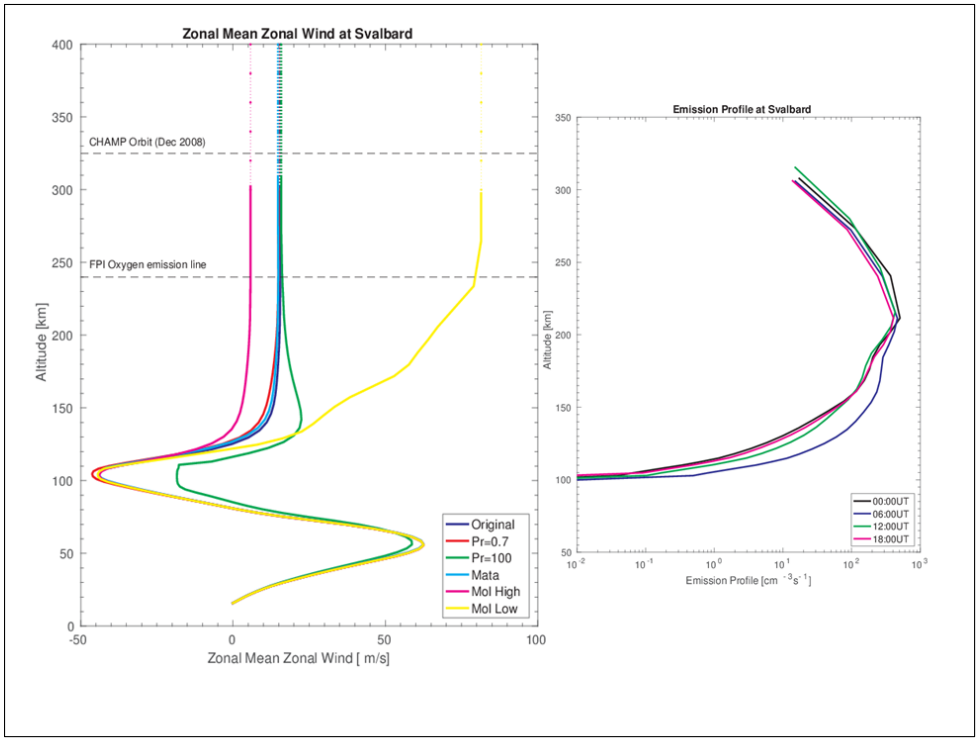

Figure 11 illustrates how ground-based FPIs make measurements of the neutral winds at 240 km altitude. The left plot shows a height profile of the CMAT2 zonal winds at Longyearbyen. On the right is a height profile of the 630 nm (red) line emission intensity based on the Vlasov et al. (2005) model. The red line emission at night is dominated by dissociative recombination of molecular oxygen (O_2^+ + e -> O* + O) (e.g. Vlasov et al., 2005). The ground-based FPI measures the Doppler shift of the gas, height integrated through a volume along the line-of-sight. This means that all winds at all altitudes contribute to the measurement, but are weighted by the red line emission intensity. The emission height profile shows a sharp velocity gradient below 200 km, but owing to quenching of the emission through collisions, there is little emission below 200 km (note the emission intensity x-axis is a log scale), and therefore a minimal contribution to the height-integrated line-of-sight wind measurement. Above 200 km the wind magnitudes begin to reach an asymptote. It therefore would be expected that the satellites and ground-based FPIs should see very similar speeds and phases. The tristatic FPI experiments by Aruliah et al (2005) and bistatic experiments by Anderson et al (2012) indicated that the winds, neutral temperatures and 630 nm intensities were closely matched if the geometry assumed an emission altitude of around 240 km. However, during auroral activity, when there is E-region precipitation, the red line emission altitude can be lower, perhaps as low as 200 km. This means that the FPI samples lower altitudes. Recently Gillies et al. (2017) used all-sky imagers to triangulate the peak emission height of the 630 nm emission. They found that discrete auroral arcs showed a characteristic height of 200km. The effect of particle precipitation in lowering the emission height was earlier noted by Sica et al. (1986). They illustrated how decreased

Ann. Geophys. Discuss., https://doi.org/10.5194/angeo-2019-57
Manuscript under review for journal Ann. Geophys.
Discussion started: 29 April 2019

thermospheric temperatures measured by a Fabry-Perot spectrometer at College, Alaska, were consistent with lower MSIS temperatures (Hedin et al., 1977) when weighted by a modelled emission height profile. However, aurorae are limited to high latitudes and occur infrequently as illustrated by Figure 12, which shows the frequency distributions of Kp values for the years (top) 2001-2003 representing solar maximum; and (bottom) 2000-2009, i.e., for most of the period of the CHAMP lifetime. Aurora generally occur during active periods when Kp > 4-5. Thus emission heights of 200 km are the exception rather than the rule.

Fig 12 Frequency distribution of Kp values. Top: 2001-2003 representing solar maximum. Bottom: 2000-2009 covering most of the period of the CHAMP lifetime.

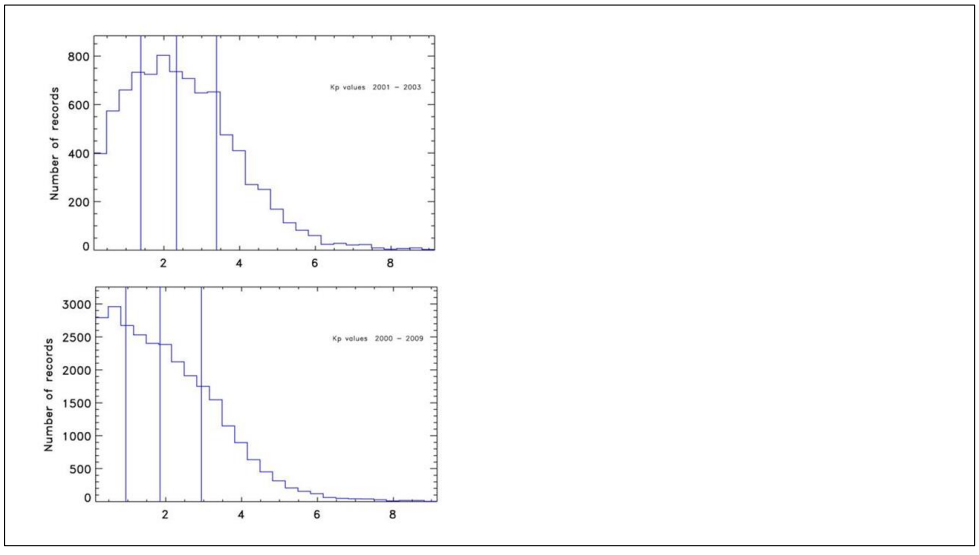

Ann. Geophys. Discuss., https://doi.org/10.5194/angeo-2019-57
Manuscript under review for journal Ann. Geophys.
Discussion started: 29 April 2019

Annales Geophysicae Discussions
Open Access
EGU

Fig 13 top: CMAT2 zonally averaged zonal winds for a quiet day on 1st December 2007 at Longyearbyen (left) and Kiruna (right) for the winds at 180, 200 and 240km for comparison with the height integrated winds weighted using an emission intensity profile from the Vlasov et al (2005) model. Bottom: the same for active conditions on 20th March 2015.

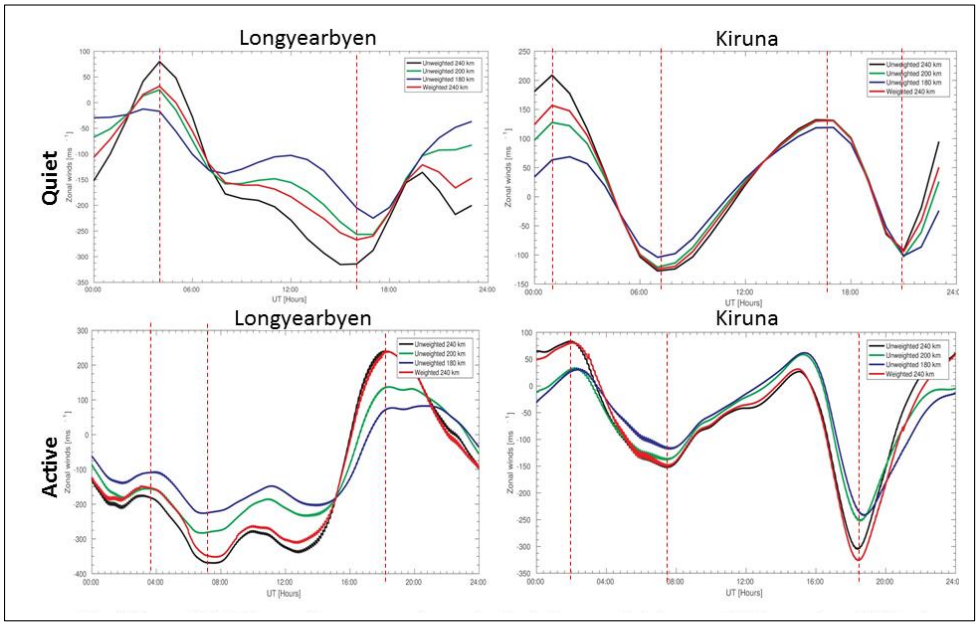

In order to assess by how much the FPI height integration method is underestimating winds, CMAT2 winds at 240 km are compared to a column integration average of CMAT2 winds weighted by the emission intensity profile. Here the Vlasov et al (2005) model is applied with constants provided by Yiu (2014), and with CMAT2 winds interpolated to 10 km intervals for the integration. Figure 13 compares the CMAT2 zonally averaged zonal winds at three heights: 180 (blue), 200 (green) and 240 km (black) with height integrated winds (red) for a quiet day run on the 1st December 2007 (top panels) and an active day run on the 20th March 2015 (bottom panels) for both Longyearbyen (left column) and Kiruna (right column). Figure 14 outlines the CMAT2 model global view of the unweighted and weighted winds at 240km for 00, 06, 12 and 18UT.

Ann. Geophys. Discuss., https://doi.org/10.5194/angeo-2019-57
Manuscript under review for journal Ann. Geophys.
Discussion started: 29 April 2019

Annales Geophysicae Discussions
Open Access
EGU

671 **Fig 14:CMAT2 global zonal winds for a quiet day on 1st December 2007 for the winds at 240km and the height**
672 **integrated winds weighted using an emission profile from Vlasov et al (2005) model. From top left: 0UT, 6UT. From**
673 **bottom left: 12UT, 18UT.**

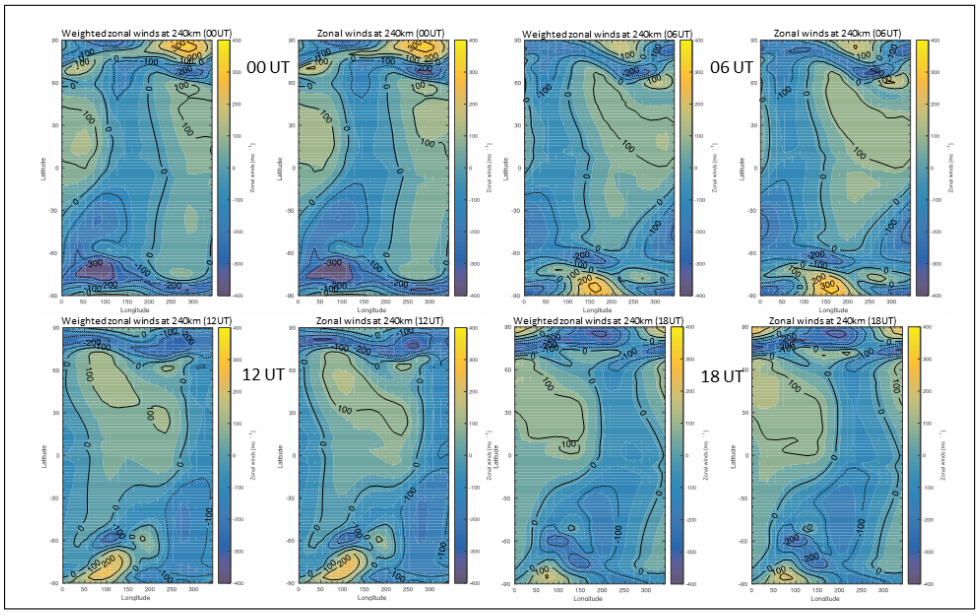

674

675 Figure 13 indicates that there are some significant differences between zonally averaged zonal winds with or
676 without height integration. The lower the altitude, the smaller the wind magnitude. There is also a slight change
677 in phase (to aid the eye these are indicated by vertical dashed lines placed at turning points for the weighted
678 winds). This is due to the increased collision frequency at lower altitudes due to greater density, and the
679 consequent shift in balance between pressure gradient and ion drag. When we look at the averaged diurnal
680 variation of the CHAMP and FPI winds, their phases are almost exactly the same. This would not be the case if
681 the FPI was observing winds dominated by Doppler shifts at 190km altitude, where the phase would be different
682 because the pressure gradient increases its dominance at lower altitudes. Comparing the CMAT2 December
683 2007 model zonally averaged zonal winds at 240 km with the height integrated winds, the most significant
684 difference is for Longyearbyen during quiet conditions, which on calculating overall mean values produces a
685 19% difference, that during active conditions reduces to a difference of 12%. The reverse seems the case for
686 Kiruna as the mean percentage difference increases from 3% to 14% between the quiet and active days
687 respectively. Note that the wind speed scales are different for each panel. For each time-series there is no simple
688 systematic trend. Figure 14 demonstrates these dissimilarities on a global scale; here the zonal winds appear to
689 be slightly more westward, as the Eastward winds are diminished and the Westward winds enhanced. However,
690 this is not the case for all times of day shown here, and is not visibly affecting the wind distributions to a large
691 extent.

692

Ann. Geophys. Discuss., https://doi.org/10.5194/angeo-2019-57
Manuscript under review for journal Ann. Geophys.
Discussion started: 29 April 2019

6.3 CHAMP cross track wind procedure

Satellites have provided global coverage of accelerometer measurements since 2001, in particular, the CHAMP satellite (e.g. Schlegel et al., 2005) and GRACE satellites (e.g. Tapley et al., 2004). These measurements of satellite drag have been converted to measurements of thermospheric density (e.g. Liu et al., 2005) and cross-track thermospheric wind measurements (e.g. Sutton et al, 2007, Liu et al., 2006, Förster et al., 2008) using Eq. 6, where $\underline{a}$ is the satellite acceleration, ρ the neutral mass density of the air, C_d refers to a dimensionless drag coefficient, using a constant frontal area A_{ref} of the satellite with mass m, and total velocity V relative to the atmosphere in the ram direction given by the unit vector $\underline{\hat{v}}$.

$$\underline{a} = -\frac{1}{2}\rho\frac{C_d}{m}A_{ref}V^2\underline{\hat{v}} \quad (6)$$

For the first analysis, Liu et al. (2005) explained that they used a fixed drag coefficient value of $C_d = 2.2$. This is a de-facto standard value used for compact satellite orbit computations since the 1960s (e.g. Cook, 1965). This value was adopted by Jacchia when constructing his thermosphere density model, based on physical drag modelling of spherical satellites (Jacchia and Slowey, 1972). The drag coefficient is acknowledged to be very difficult to quantify, as is discussed extensively by, for example, Moe et al. (1995). The importance of the value of C_d is acknowledged by Liu et al (2006) and others who use the data, since it affects the scaling of the density and wind calculations. However, their interest was in the relative density and wind structures, rather than absolute values. Since then the analysis has been refined considerably by taking into account lift, sideways, as well as drag forces on the satellite, resulting in smaller wind magnitudes as described by Doornbos et al. (2010). The GOCE satellite winds are closer in magnitude to ground-based FPI measurements (Dhadly et al., 2017), though still systematically larger in magnitude, where the difference has been found to increase with latitude. The systematic residual line-of-sight GOCE wind varied between 20 ms^{-1} at 50° MLAT to a maximum 150 ms^{-1} at 85° MLAT (see Figure 2 from Dhadly et al., 2018).

Another consideration is that CHAMP measures the cross-track wind component (Figures 1 and 2) which deviates from the pure zonal direction as measured by the FPIs (Figures 3 and 4). The geometry can be critical, in particular for the high-latitude Longyearbyen FPI, because the cross-track deviates from the zonal direction by about 13.5° in each direction respectively for the ascending and descending orbits. The meridional wind component at these high latitudes is much larger than the zonal one, so that the larger CHAMP measurements at this FPI could also (at least partially) be due to an "admixture" of the meridional wind component and the zonal wind. This has been discussed in section 5.1 to account for the difference between the average zonal winds measured during the ascending and descending orbits.

6.4 Comparison with EISCAT radar ion velocities

Finally, a very important consideration is how the average winds compare with ion velocities. At high latitudes the ion velocities are generally larger than the neutral winds owing to the ExB drift driven by the magnetospheric electric field. Davies et al (1995) provided a statistical analysis of E- and F- region ion

velocities observed on 20 March 1996 in order to compare measurements by the EISCAT incoherent scatter radars and the CUTLASS coherent scatter radar. The scatter plot of ion velocities from this study (their Figure 5) indicated a cluster of values in the range of a few hundred ms^{-1}, with only a small fraction of measurements greater than 500 ms^{-1}.

Fiori et al (2016) compared ion velocities measured by the Electric Field Instrument on Swarm with the CS10 statistical ionospheric convection model by Cousins and Shepherd (2010) which is based on 8 years of data (1998-2005) collected by 16 SuperDARN coherent scatter radars. The climatology represented by the CS10 model in Fiori et al's Figure 3a indicates speeds in the few hundreds of ms^{-1}, while the instantaneous values along the Swarm satellite pass in their Fig 3d show horizontal velocities over a 1000 ms^{-1}, which probably indicates the dynamic behaviour in the auroral regions.

Aruliah et al. (1996) presented the seasonal and solar cycle variation of hourly averaged ion velocities from 300 days of EISCAT Tromsø UHF radar measurements between 1984-1990. The tristatic EISCAT radar observations for an altitude of 275 km were collected from Common Programmes 1, 2 and 3, at time resolutions of 2-3 mins, with full 24 hours coverage. The ion velocities for December solstice periods were up to 100-200 ms^{-1}, and the largest average ion velocities were around 300 ms^{-1} during the March equinox period at solar maximum. Aruliah et al. (2005) later reported observations of a common volume using a configuration of tristatic FPI observations of the thermospheric winds and temperatures co-located with tristatic EISCAT radar measurements of ionospheric parameters at 250 km altitude. The observations showed that the neutral winds were on average around 50% of the magnitude of the 15 min average ion velocities.

Griffin et al. (2004) determined seasonal and solar cycle climatologies of meridional winds at Kiruna using FPI Doppler shifts, and derived from field-aligned ion velocities (Salah and Holt, 1974), which were compared with physical (CTIM, Fuller-Rowell et al., 1988) and empirical models (HWM, Hedin et al, 1988; MWM, Miller et al., 1997). The climatologies all showed meridional winds up to ~250 ms^{-1}. Although this method does not give the zonal wind magnitude, it gives some indication of typical magnitudes owing to the diurnal variation of winds seen by a single site as the Earth rotates.

Förster et al. (2008) presented a statistical comparison of observed averaged neutral wind velocities within the polar cap (magnetic latitudes > 80°) for the year 2003 showing the dependence on the IMF orientation based on statistical analyses of CHAMP accelerometer data with average ion drift estimates for the same time interval and IMF conditions based on EDI Cluster measurements. These comparisons were done for both the Northern and the Southern Hemisphere separately in their Tables 1 and 2, respectively. Depending on the IMF clock angle orientation, the ratio between average neutral wind magnitudes and average ion drift speeds varies between about 60% and around 100%. Interestingly, there is a characteristic interhemispheric difference with respect to the IMF orientation and slightly larger ion drift velocities on average in the Northern Hemisphere (cf. Förster and Cnossen, 2013; Förster et al., 2017), but the overall average amounts to a ratio of about 0.90 to 0.95 for, note well, within the polar cap region > 80° magnetic only. The FPI in Longyearbyen at 75.4° N (see Table 2) comes closest to this region. Ion drag is the dominating forcing term here for the neutral gas, while near the auroral ring, where the KEOPS FPI station in Kiruna at 65.1° N is located, the balance between the different forces, in particular pressure gradient terms, Coriolis and centrifugal forces, and ion drag play a role. There the

ratio between the average neutral wind and ion drag magnitudes is certainly smaller, corresponding to the EISCAT observations cited above.

7 Conclusions

A comparison is presented here of thermospheric zonal winds measured by the CHAMP satellite in the altitude region 350-400 km, and by ground-based FPIs, at Kiruna and Longyearbyen, measured at about 240 km altitude. The satellite accelerometer measurements are used to derive cross-track winds, while the FPIs use the Doppler shift of the 630 nm emission. The satellite measurements are collected for a region within 2° of the FPI sites, which is within the field of view of the FPI East and West look directions. The phases of the winds agree very well, but the CHAMP average zonal winds are a factor 1.5-2.0 larger than the FPI average zonal winds. The factor is not simple. In particular there is a difference in the factor for the auroral site and the polar cap site, so it appears that the factor is dependent on location, possibly latitude.

The UCL Longyearbyen FPI winds are consistent with FPI measurements made 20 years previously by the University of Alaska using a different FPI and detector (photometer in 1980, EMCCD in 2001). Earlier studies of average ion velocities from the EISCAT Tromsø UHF radar compared with the UCL FPI at KEOPS indicate that in the auroral zone the average ion velocities are about twice the average neutral wind speeds (Aruliah et al., 1996 and 2005). However, the CHAMP average KEOPS zonal winds presented here have magnitudes similar to the average *ion* velocities of the December solstice values presented by Aruliah et al (1996). It is important to determine the absolute wind values since the difference between the ion and neutral winds determine the amount of Joule heating of the thermosphere.

Satellites play a crucial role in upper atmosphere research by filling in the extensive gaps between ground-based observations. Satellites provide 3-dimensional coverage at high spatial resolution, in addition to high temporal resolution. Meanwhile, ground-based instruments are sparse, land-based, and not always operational on a 24/7 basis owing to operational costs (e.g. incoherent scatter radars) or observing constraints (e.g. only night-time and clear sky observations for optical instruments). Having uncovered this discrepancy between ground-based FPI optical measurements and satellite drag measurements of winds, it is imperative to determine if it is a real altitude dependence, or if some re-scaling of winds, is necessary for winds determined from either, or both, of FPI height-integrated Doppler shifts or satellite drag measurements. Both will affect our current modelling of the upper atmosphere; or whether we need to rethink the procedure of comparing different spatial and temporal resolutions of in-situ satellite versus remote ground-based FPI measurements and the geometry of cross-track winds at high latitude.

Author contributions. This paper is the result of many years of collaboration between AA and MF after noticing the significant difference between FPI and CHAMP winds. AA provided the FPI data, MF provided the CHAMP data. RH provided the model simulations, IM provided technical support for the FPIs, and ED provided expertise on converting accelerometer data to winds.

Competing interests. The authors declare that they have no conflict of interest

*Acknowledgements***.** We thank the staff at the Kjell Henriksen Observatory and ESRANGE for hosting the FPIs and their generous on-site assistance. Support for the FPI operations have come from the European Office of Aerospace Research and Development (grant FA9550-17-1-0019). There has been NERC support of ALA (grants NE/P001556/1 and NE/N004051/1). The CHAMP mission is sponsored by the Space Agency of the German Aerospace Center (DLR) through funds of the Federal Ministry of Economics and Technology, following a decision of the German Federal Parliament (grant code 50EE0944). The data retrieval and operation of the CHAMP satellite by the German Space Operations Center (GSOC) of DLR is acknowledged. EISCAT is an international association supported by research organisations in China (CRIRP), Finland (SA), France (CNRS, till end 2006), Germany (DFG), Japan (NIPR and STEL), Norway (NFR), Sweden (VR), and the United Kingdom (STFC). We also acknowledge support from the International Space Science Institute for sponsoring meetings of the international team #308 on 'M-I-T Coupling: Differences and similarities between the two hemispheres', which helped this collaboration (http://www.issibern.ch/teams/twohemispheres/).

References:

Anderson, C., Conde, M., and McHarg, M. G.: Neutral thermospheric dynamics observed with two scanning Doppler imagers: 1. Monostatic and bistatic winds, J. Geophys. Res.,117, A03304, doi:10.1029/2011JA017041, 2012.

Aruliah A.L., Rees, D.: The Trouble with Thermospheric Vertical Winds: Geomagnetic, Seasonal and Solar Cycle Dependence at High Latitudes, J. Atmos. Terr. Phys., 57, 597-609, 1995

Aruliah A.L., Farmer, A. D., Rees, D., Brändström, U.: The Seasonal Behaviour of High-Latitude Thermospheric Winds and Ion Velocities Observed Over One Solar Cycle, J. Geophys. Res., 101, 15701-15711, 1996

Aruliah, A. L. and Griffin, E. M.: Evidence of meso-scale structure in the high-latitude thermosphere, Ann. Geophys., 37–46, 2001.

Aruliah, A. L., Griffin, E. M., Aylward, A. D., Ford, E. A. K., Kosch, M. J., Davis, C. J., Howells, V. S. C., Pryce, E., Middleton, H., Jussila, J.: First direct evidence of meso-scale variability on ion-neutral dynamics using co-located tristatic FPIs and EISCAT radar in Northern Scandinavia, EISCAT workshop special issue Annales Geophys., 23, 147-162, 2005

Bauer, S.J.: Physics and chemistry in space, Vol 6 of Physics of planetary ionospheres, Springer-Verlag, 1973

Banks, P.M. and Kockarts, G.: Aeronomy: Parts A and B. Academic Press: New York, 1973

Bruinsma, S. L., Doornbos, E., Bowman, B.R.: Validation of GOCE densities and evaluation of thermosphere models Advances in Space Research, Volume 54, Issue 4, 576-585.10.1016/j.asr.2014.04.008, 2014.

Cook, G.E.: Satellite drag coefficients, Planet. Space Sci., 13, 929, 1965

Dalgarno, A., and Smith, F. J.: The thermal conductivity and viscosity of atomic oxygen, Planet.Space.Sci., 9, 1-2, 1962.

Davies, J.A., Lester, M., Milan, S.E., Yeoman, T. K.: A comparison of velocity measurements from the CUTLASS Finland radar and the EISCAT UHF system, Ann.Geophys., 17, 892-902, 1999.

842 Deehr, C. S., Sivjee, G. G., Egeland, A., Henriksen, K., Sandholt, P. E., Smith, R., Sweeney, P., Duncan, C.,
843 Gilmer, J.: Ground-based observations of F region aurora associated with the magnetospheric cusp, J.
844 GEOPHYS. RES., 85, 2185-2192, 10.1029/JA085iA05p02185, 1980.
845 Dhadly, M., Emmert, J., Drob, D., Conde, M., Doornbos, E., Shepherd, G., Makela, J., Wu, Q., Niciejewski, R.,
846 and Ridley, A.: Seasonal dependence of northern high-latitude upper thermospheric winds: A quiet time
847 climatological study based on ground-based and space-based measurements, Journal of Geophysical
848 Research (Space Physics), 122, 2619-2644, 10.1002/2016JA023688, 2017
849 Dhadly, M., Emmert, J., Drob, D., Conde, M., Shepherd, G., Makela, J., Wu, Q., Niciejewski, R., and Ridley,
850 A.: Seasonal Dependence of geomagnetic active-time northern high-latitude upper thermospheric winds, J.
851 GEOPHYS. RES., 123, 739-754, https://doi.org/10.1002/2017JA024715, 2018
852 Doornbos, E, Ijssel, J., Lühr, H., Förster, M., and Koppenwallner, G:. Neutral density and crosswind
853 determination from arbitrarily oriented multiaxis accelerometers on satellites. Journal of Spacecraft and
854 Rockets, 47(4): 580–589, 2010. doi:10.2514/1.48114, 2010
855 Drob, D. P., Emmert, J. T., Meriwether, J. W., Makela, J. J., Doornbos, E, Conde, M., Hernandez, G., Noto, J.,
856 Zawdie, K. A., McDonald, S. E., Huba, J. D., and Klenzing, J. H.: An update to the Horizontal Wind Model
857 (HWM): The quiet time thermosphere, Earth and Space Science, 2, 301-319, 10.1002/2014EA000089,
858 https://doi.org/10.1002/2014EA000089,2015
859 Emmert, J. T., Faivre, M. L., Hernandez, G., Jarvis, M. J., Meriwether, J. W., Niciejewski, R. J., Sipler, D. P.,
860 and Tepley, C. A.: Climatologies of nighttime upper thermospheric winds measured by ground-based Fabry-
861 Perot interferometers during geomagnetically quiet conditions: 1. Local time, latitudinal, seasonal, and solar
862 cycle dependence, J. Geophys. Res., 111, A12302, doi:10.1029/2006JA011948, 2006a
863 Emmert, J.T., Hernandez, G., Jarvis, M. J., Niciejewski, R. J., Sipler, D. P., and Vennerstrom, S.: Climatologies
864 of nighttime upper thermospheric winds measured by ground-based Fabry-Perot interferometers during
865 geomagnetically quiet conditions: 2. High-latitude circulation and interplanetary magnetic field dependence,
866 J. Geophys. Res., 111, A12303, doi:10.1029/2006JA011949, 2006b.
867 Fiori, R. A. D., Koustov, A. V., Boteler, D. H., Knudsen, D. J., & Burchill, J. K.: Calibration and assessment of
868 Swarm ion drift measurements using a comparison with a statistical convection model. Earth, Planets and
869 Space, 68(1), 100. http://doi.org/10.1186/s40623-016-0472-7, 2016.
870 Forbes, J. M., Roble, R. G., and Marcos, F. A.: Magnetic activity dependence of high–latitude thermospheric
871 winds and densities below 200 km, J. Geophys. Res., 98, 13,693–13,702, 1993.
872 Ford, E.A.K., Aruliah, A.L., Griffin, E.M., McWhirter, I.: High time resolution measurements of the
873 thermosphere from Fabry-Perot Interferometer measurements of atomic oxygen, Annales Geophys., 25,
874 1269 – 1278, 2007.
875 Förster, M., Rentz, S., Köhler, W., Liu, H., and Haaland, S. E.: IMF dependence of high-latitude thermospheric
876 wind pattern derived from CHAMP cross-track measurements, Ann. Geophys., 26, 1581–1595, 2008.
877 Förster, M., Haaland, S.E., and Doornbos, E., Thermospheric vorticity at high geomagnetic latitudes from
878 CHAMP data and its IMF dependence, Ann. Geophys., 29, 181-186, doi:10.5194/angeo-29-181-2011, 2011.
879 Förster, M., and Cnossen, I.: Upper atmosphere differences between northern and southern high latitudes: The
880 role of magnetic field asymmetry, J. Geophys. Res. Space Physics, *118*, 5951–5966,
881 doi:10.1002/J.Geophys.Res.a.50554, 2013.

Förster, M., Doornbos, E., and Haaland S.: The role of the upper atmosphere for dawn-dusk differences in the coupled magnetosphere-ionosphere-thermosphere system", in: Dawn-Dusk Asymmetries in Planetary Plasma Environments, eds. Stein Haaland, Andrei Runov and Colin Forsyth, John Wiley Publications, AGU Geophysical Monograph, Vol. 230, 125-142, ISBN: 978-1-119-21632-2, 2017.

Foster, J. C., Holt, J. M., Musgrove, R. G., and Evans, D. S.: Ionospheric convection associated with discrete levels of particle precipitation, Geophys. Res. Lett., 13, 656, 1986.

Fuller-Rowell, T. J.: Modelling the solar cycle change in nitric oxide in the thermosphere and upper mesosphere, J. Geophys. Res., 98, 1571, 1992.

Fuller-Rowell, T.J., Rees, D.: Interpretation of an Anticipated Long-Lived Vortex in the Lower Thermosphere Following Simulation of an Isolated Substorm, Planet. Space Sci., 32, 69-85, 1984

Fuller-Rowell T.J., Evans, D.S.: Height Integrated Pedersen and Hall Conductivity Patterns Inferred from the TIROS-NOAA Satellite Data, J. GEOPHYS. RES., 92, 7606-7618, 1987

Fuller-Rowell, T. J., Rees, D., Quegan, S., Moffett, R. J., Bailey, G.J.: Simulations of the seasonal and UT variations of the thermosphere and ionosphere using a coupled, three-dimensional, global model, Pur. A. Geoph., 127, 189–217, 1988.

Fuller-Rowell, T. J., Rees, D., Quegan, S., Moffett, R. J., Codrescu, M. V., and Millward, G. H.: A coupled thermosphere ionosphere model, Solar terrestrial energy program (STEP), handbook of ionospheric models, (Ed) Schunk, R. W., 1996.

Gillies, M. D., Knudsen, D., Donovan, E., Jackel, B., Gillies, R., Spanswick, E.: Identifying the 630 nm auroral arc emission height: A comparison of the triangulation, FAC profile, and electron density methods, J. Geophys. Res. Space Physics, 122, doi:10.1002/2016JA023758, 2017.

Griffin, E.M., Aruliah, A. L., Müller-Wodarg, I. C. F., Aylward, A. D.: Comparison of High-Latitude Thermospheric Meridional Winds II: Combined FPI, Radar and Model Climatologies, Ann. Geophys, 22, 863-876, 2004.

Griffin, E. M., Müller-Wodarg, I. C. F., Aruliah, A., and Aylward, A.: Upper thermospheric neutral wind and temperature measurements from an extended spatial field, Ann. Geophys., 26, 2649– 2655, 2008.

Harang, L.: The mean field of disturbance of polar geomagnetic storms, Terr. Mag. Atmos. Elec., 51, 353-380, 1946.

Harris, M.: A New Coupled Middle Atmosphere and Thermosphere General Circulation Model: Studies of Dynamic, Energetic and Photochemical Coupling in the Middle and Upper Atmosphere. PhD Thesis, London, 2017.

Harris, M. J., Arnold, N. F., and Aylward, A. D.: A study into the effect of the diurnal tide on the structure of the background mesosphere and thermosphere using the new coupled middle atmosphere and thermosphere (CMAT) general circulation model, Ann. Geophys., 20, 225–235, doi:10.5194/angeo-20-225-2002, 2002.

Hecht, E., Zajac, A.: Optics, Addison-Wesley Publishing Company, 1980.

Hedin A. E., Salah, J. E., Evans, J. V., Reber, C. A., Newton, G. P., Spencer, N. W., Kayser, D. C., Alcayde, D., Bauer, P., Cogger, L., McClure, J. P.: A Global Thermospheric Model Based on Mass Spectrometer and Incoherent Scatter Data MSIS 1. N_2 Density and Temperature, J.Geophys.Res., 82, 2139-2147, 1977.

Hedin A.E., Biondi, M. A., Burnside, R. G., Hernandez, G., Johnson, R. M., Killeen, T. L., Mazaudier, C., Meriwether, J. W., Salah, J. E., Sica, R. J., Smith, R. W., Spencer, N. W., Wickwar, V. B., Virdi, T. S.:

Revised Global Model of Thermospheric Winds Using Satellite and Ground-Based Observations, J. Geophys. Res. Space Physics, 96, 7657-7688, 1991.

Helleputte, T. V., Doornbos, E., and Visser, P.: CHAMP and GRACE accelerometer calibration by GPS-based orbit determination. Advances in Space Research, 43(12), 1890–1896. http://doi.org/10.1016/j.asr.2009.02.017, 2009.

Jacchia, L. G., and Slowey, J. W.: A supplemental catalog of atmospheric densities from satellite-drag analysis (No. 348). SAO Special Report, 1972.

Killeen, T. L., Smith, R. W., Hays, P. B., Spencer, N. W., Wharton, L. E., McCormac, F. G.: Neutral winds in the high latitude winter F-region: Coordinated observations from ground and space, Geophys. Res. Lett., 11, 311-314, 1984.

Killeen T.L., Won, Y.-I., Niciejewski, R.J., Burns, A.G.: Upper Thermosphere Winds and Temperatures in the Geomagnetic Polar Cap: Solar Cycle, Geomagnetic Activity and IMF Dependencies, J. Geophys. Res., 100, 21327-21342, 1995.

Link, R., Cogger, L.L.: A re-examination of the O I 6300A nightglow, J. Geophys. Res., 93, 9883-9892, 1988.

Liu, H., Lühr, H., Henize, V., and Köhler, W.: Global distribution of the thermospheric total mass density derived from CHAMP, J. Geophys. Res., 110, A04301, doi:10.1029/2004JA010741, 2005.

Liu, H., Lühr, H.,Watanabe, S., Köhler,W., Henize, V., and Visser, P.: Zonal winds in the equatorial upper thermosphere: Decomposing the solar flux, geomagnetic activity, and seasonal dependencies, J. Geophys. Res., 111, A07307, doi:10.1029/2005JA011415, 2006.

Liu, H., Doornbos, E., & Nakashima, J.: Thermospheric wind observed by GOCE: Wind jets and seasonal variations. Journal of Geophysical Research: Space Physics, 121(7), 6901–6913. http://doi.org/10.1002/2016JA022938, 2016.

Makela, J. J., Meriwether, J. W., Huang, Y., Sherwood, P. J.: Simulation and analysis of a multi-order imaging Fabry-Perot interferometer for the study of thermospheric winds and temperatures, Applied Optics, 50, 4403-4416, 2011.

March, G., Doornbos, E. N. and Visser, P. N. A. M.: High-fidelity geometry models for improving the consistency of CHAMP, GRACE, GOCE and Swarm thermospheric density data sets, Advances in Space Research, 63, 213-238, 10.1016/j.asr.2018.07.009, 2018.

Marcos, F. A. and Forbes, J. M.: Thermospheric wind from the satellite electrostatic triaxial accelerometer system, J. Geophys. Res., 90, 6543–6552, 1985.

McWhirter I., Rees, D., Greenaway, A. H.: Miniature Imaging Photon Detectors III.~An Assessment of the Performance of the Resistive Anode IPD, J. Phys. E.: Sci. Instrum., 15, 145-150, 1982.

McWhirter, I., Electron Multiplying CCDs - New Technology for Low Light Level Imaging, Proceedings of 33rd Annual European Meeting on Atmospheric Studies by Optical Methods, IRF Sci. Rep., 292, 61-66, 2008.

Mehta, P. M., Walker, A. C., Sutton, E., & Godinez, H. C.: New density estimates derived using accelerometers on-board the CHAMP and GRACE satellites. Space Weather, 15(4), 558–576. http://doi.org/10.1002/2016SW001562, 2017.

Moe, Mildred. M., Wallace, Steven D., Moe, Kenneth : The upper mesosphere and lower thermosphere, A review of experiment and theory, Geophysical Monograph 87, 1995

962 Quegan, S., Bailey, G. J., Moffett, R. J., Heelis, R. A., Fuller-Rowell, T. J., Rees, D., and Spiro, A. W.: A
963 theoretical study of the distribution of ionisation in the high-latitude ionosphere and the plasmasphere: First
964 results of the mid-latitude trough and the light ion trough, J. Atm. Terr. Phys., 44, 619, 1982.
965 Rees, D., Fuller-Rowell, T. J., Gordon, R., Smith, M. F., Maynard, N. C., Heppner, J. P., Spencer, N. W.,
966 Wharton, L., Hays, P. B., and Killeen, T. L.: A theoretical and empirical study of the response of the high
967 latitude thermosphere to the sense of the "Y" component of the interplanetary magnetic field, Planet. Space
968 Sci., 34, 1–40, 1986.
969 Reigber, C., Lühr, H., and Schwintzer, P.: CHAMP mission status, Adv. Space Res., 30, 129–134, 2002.
970 Roble, R. G., Ridley E. C., and Dickenson, R. E.: On the global mean structure of the thermosphere, J. Geophys.
971 Res., 92, A8, 8745–8758, 1987.
972 Ronksley, Amy, Optical remote sensing of mesoscale thermospheric dynamics above Svalbard and Kiruna, PhD
973 thesis, UCL, London, UK., 2016.
974 Salah, J. E. and Holt, J. M.: Midlatitude thermospheric winds from incoherent scatter radar and theory, Radio
975 Sci., 9, 301–313, 1974.
976 Schlegel, K., Lühr, H., St.-Maurice, J.-P., Crowley, G., and Hackert, C.: Thermospheric density structures over
977 the polar regions observed with CHAMP, Annales Geophysicae, 23, 1659–1672, 2005.
978 Shepherd, S. G.: Altitude-adjusted corrected geomagnetic coordinates: Definition and functional
979 approximations, J. Geophys. Res. Space Physics, 119, doi:10.1002/2014JA020264, 2014.
980 Sica R. J., Rees, M. H., Roble, R. G., Hernandez, G., Romick, G. J.: The Altitude Region Sampled by Ground-
981 Based Doppler Temperature Measurements of the OI 15867K Emission Line in Aurorae, Planet. Space Sci.,
982 34, 483-488, 1986.
983 Smith, R. W., Sweeney, P. J.: Winds in the thermosphere of the northern polar cap, Nature **284**, 437 – 438,
984 doi:10.1038/284437a0, 1980.
985 Song, P., Vasyliūnas, V. M., and Zhou, X.-Z.: Magnetosphere-ionosphere/thermosphere coupling: Self-
986 consistent solutions for a one-dimensional stratified ionosphere in three-fluid theory, J. Geophys. Res., 114,
987 A08213, doi:10.1029/2008JA013629, 2009.
988 Song, P., and Vasyliūnas, V. M.: "Inductive-dynamic coupling of the ionosphere with the thermosphere and the
989 magnetosphere", in: 'Modeling the Ionosphere-Thermosphere System', edited by J. Huba, R. Schunk, and G.
990 Khazanov, American Geophysical Union, Washington DC,10.1029/2012GM001308, Geophysical
991 Monograph Series 201, 201-215, 2013.
992 Sutton, E. K., Nerem, R. S., & Forbes, J. M.: Density and Winds in the Thermosphere Deduced from
993 Accelerometer Data. Journal of Spacecraft and Rockets, 44(6), 1210–1219. http://doi.org/10.2514/1.28641,
994 2007.
995 Tapley, B.D., Bettadpur, S., Watkins, M., and Reigber, C.: The gravity recovery and climate experiment:
996 Mission overview and early results, Geophys. Res. Lett., 31, L09607, DOI: 10.1029/2004GL019920, 2004.
997 Torr, M. R., Richards, P. G., and Torr, D. G.: A new determination of ultraviolet heating efficiency in the
998 thermosphere, J. Geophys.Res., 85, 6819, 1980a.
999 Torr, M. R., Richards, P. G., and Torr, D. G.: The solar ultraviolet heating efficiency in the mid-latitude
1000 thermosphere, Geophys.Res. Lett., 6, 673, 1980b.

1001 Vadas, S. L. and Crowley, G.: Neutral wind and density perturbations in the thermosphere created by gravity
1002 waves observed by the TIDDBIT sounder, J. Geophys. Res. Space Physics, *122*, 6652–6678,
1003 doi:10.1002/2016JA023828, 2017.
1004 Visser, T., March, G., Doornbos, E., de Visser, C., & Visser, P.: Horizontal and vertical thermospheric cross-
1005 wind from GOCE linear and angular accelerations. Advances in Space Research.
1006 http://doi.org/10.1016/j.asr.2019.01.030, 2019.
1007 Vlasov, M. N., Nicolls, M. J., Kelley, M. C., Smith, S. M., Aponte, N., and Gonzalez, S. A: Modeling of
1008 airglow and ionospheric parameters at Arecibo during quiet and disturbed periods in October 2002, J.
1009 Geophys. Res., 110, A07303, doi:10.1029/2005JA011074, 2005.
1010 Yiu, H.C.I: High latitude thermosphere meso-scale studies and long-term database investigations with the new
1011 Scanning Doppler Imager and Fabry-Perot Interferometers, Ph.D. Thesis, Univ. of London, London, UK,
1012 2014.